A Comparative Study of Principal Component Analysis (PCA) and Dynamic Mode Decomposition (DMD) Variants

Yile He

A thesis
submitted in partial fulfillment of the
requirements for the degree of

Master of Science

University of Washington

2024

Reading Committee:

Eardi Lila

Kenneth Rice

Program Authorized to Offer Degree:

Department of Biostatistics

University of Washington

Abstract

A Comparative Study of Principal Component Analysis (PCA) and Dynamic Mode Decomposition (DMD) Variants

Yile He

Chair of the Supervisory Committee:
Eardi Lila
Department of Biostatistics

This study evaluates the performance of the Exact Dynamic Mode Decomposition (DMD), Optimized DMD, and Modified Optimized DMD algorithms under various noise conditions, with a specific focus on magnetoencephalography (MEG) data. DMD is a data-driven method used to decompose complex datasets into dynamic modes, which represent the underlying structures and dynamics of the data system. We found that the Modified Optimized DMD consistently outperformed the other methods in estimating the real parts of eigenvalues that describe time dynamics, significantly reducing bias and empirical variance. Additionally, Optimized DMD and Modified Optimized DMD are able to capture more complex spatial and temporal patterns from MEG data. These results emphasize the robustness and reliability of the Modified Optimized DMD, making it a valuable tool for diverse scientific applications that require accurate dynamic mode decomposition in noisy data.

TABLE OF CONTENTS

Chapter 1

INTRODUCTION

Evaluating complex systems is a major challenge in fields like engineering, biology, and physical sciences as data collected from these systems are often high-dimensional and affected by random noise (Groun et al., 2022; Li et al., 2023; Baddoo et al., 2023). One major example is magnetoencephalography (MEG) data which is used to understand the neural activity in the brain (Brookes et al., 2022). MEG measures the magnetic fields generated by neuronal currents using a helmet-like array of superconducting sensors. These sensors detect weak magnetic fields with high temporal resolution, allowing for detailed tracking of neural dynamics. The recorded data reveals intricate patterns of brain activity as presented in Figure 1.1, and these patterns are crucial for understanding the complex and evolving interactions within the brain (Boto et al., 2018). The analysis of MEG data requires statistical methods to manage and interpret the intricate temporal and spatial patterns present in such high-dimensional datasets (Brunton et al., 2016). The challenge lies in developing methods that can effectively handle these complex dynamics, enabling researchers to gain a deeper understanding of brain function and interactions.

Dynamic Mode Decomposition (DMD) is a prominent data-driven technique for analyzing linear dynamics in high-dimensional, spatio-temporal datasets (Kutz et al., 2016). The input to DMD is a sequence of data snapshots, which are typically matrices representing the state of the system at different time points. DMD processes these snapshots to decompose the system into a set of dynamic modes and corresponding eigenvalues. The dynamic modes describe spatial patterns in the data, and the eigenvalues describe the temporal behavior associated with these modes, such as growth rates and oscillation frequencies. This method is particularly useful for applications such as fluid flows and time-series measurements (Tu,

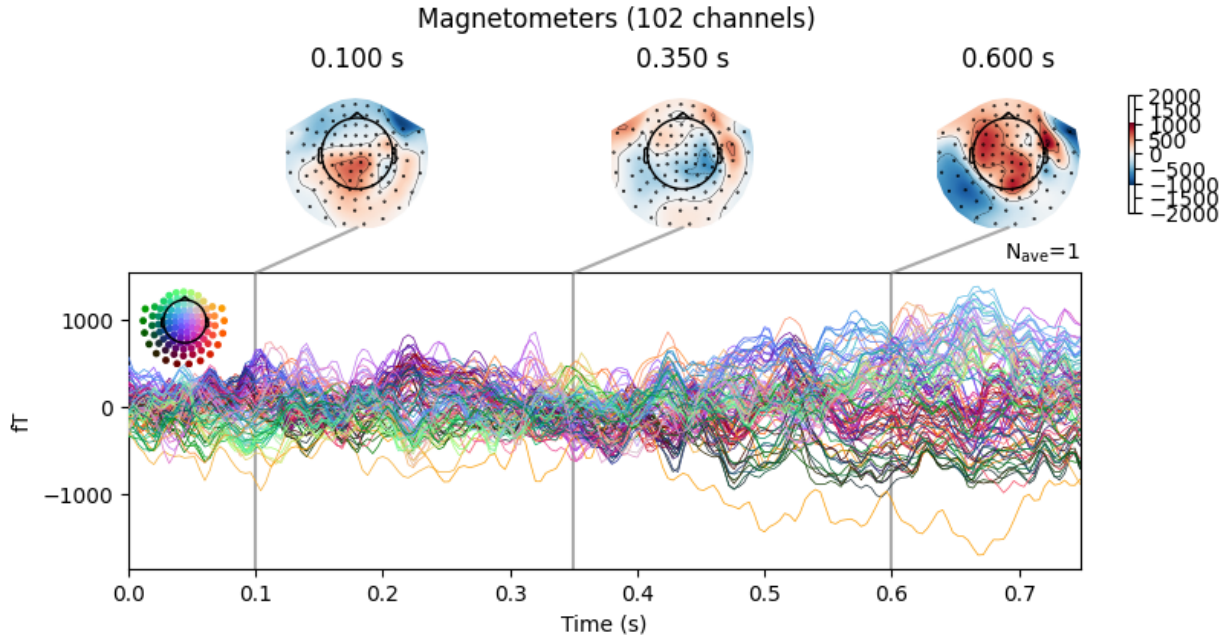

Figure 1.1: Time series data from magnetometer channels in a MEG dataset. The plot displays the magnetic field strength (fT) as a function of time in seconds (s) across 102 different channels. The insets show topographical maps of the magnetic field distribution at specific time points (0.100 s, 0.350 s, and 0.600 s), providing spatial context to the temporal data. These maps highlight areas of magnetic field strength with both positive (red) and negative (blue) values, and so in combination indicate regions of neuronal activity.

2013). In the context of MEG data, DMD is used to identify the dominant modes of brain activity and track how these modes evolve over time. However, MEG data is often contaminated by noise, which can significantly limit the effectiveness of DMD (Hemati et al., 2017). This limitation arises because DMD treats the data pairwise, snapshot-to-snapshot, and assumes a forward progression from one time point to the next instead of considering the entire dataset as a cohesive whole (Colbrook, 2023). As a result, DMD is particularly susceptible to errors introduced by noise and computes biased eigenvalue estimates, which makes it less suitable for analyzing noisy datasets.

To address these challenges, several variants of DMD have been developed. One notable variant is Optimized DMD (optDMD), which processes all data snapshots collectively rather

than sequentially (Chen et al., 2012). By fitting the data to an exponential model and solving a nonlinear optimization problem through variable projection method, Optimized DMD reduces the bias introduced by noise and effectively handles data that is not uniformly spaced in time (Golub & Pereyra, 1973). This makes it particularly useful for MEG data.

In this thesis, we introduce a modification of the Optimized DMD approach that further enhances its robustness to the presence of noise, by incorporating a debiased initial covariance estimate. This modification allows for a more accurate and robust estimation of the eigenvalues and dynamic modes. Through comprehensive evaluation and comparison with Exact DMD and Optimized DMD under different levels (low, medium, high) and types (correlated vs. uncorrelated) of noise, we demonstrate the efficiency of our modified optimized DMD approach, highlighting its potential to improve upon current state-of-the-art methods. In our final application, we apply our Modified Optimized DMD to analyze MEG data.

Given that at its core the DMD is a data decomposition method, we first review the most popular such method, Principal Component Analysis (PCA), which is designed for independent samples, and then review the main DMD methods. The rest of this thesis is organized as follows. In Chapter 2, we introduce the algorithm and interpretation of PCA, in Chapter 3 we describe different DMD methods, in Chapter 4 we compare the performance of DMD methods under different settings, and in Chapter 5 we apply the DMD methods to MEG data and compare their outputs.

Chapter 2

PRINCIPAL COMPONENT ANALYSIS (PCA)

2.1 Maximizing the variation

PCA can be viewed as a method for identifying a lower-dimensional representation of a multi-dimensional dataset, that captures the maximum possible variability within that data. Formally, first let $X \in \mathbb{R}^{n \times d}$ be a data matrix, where n is the number of observations and d is the number of variables. Then PCA seeks k components, with $k < d$ (usually $k \ll d$), that are linear combinations of the d features. Since we are only interested in variance, we assume all columns of X have been centered to zero. Let $V_1 = (V_{11}, V_{21}, ..., V_{d1})^T$ be a d-dimensional vector with unitary norm (i.e. $\sum_{i=1}^{d} V_{j1}^2 = 1$) and Z_1 be a n-dimensional vector defined as

$$Z_1 = XV_1,$$

where $Z_{i1} = V_1 1 X_{i1} + V_2 1 X_{i2} + ... + V_{d1} X_{id}$ represents the ith entry of Z_1. PCA finds the direction V_1 for which the projection of X onto V_1 (i.e. Z_1) maximises the variance retained. This is the same as solving the optimization problem

$$\underset{V_{11},...,V_{d1}}{\operatorname{argmax}} \left\{ \frac{1}{n} \sum_{i=1}^{n} \left(Z_{i1} - \bar{Z}_1 \right)^2 \right\} = \underset{V_{11},...,V_{d1}}{\operatorname{argmax}} \left\{ \frac{1}{n} \sum_{i=1}^{n} \left(\sum_{j=1}^{d} V_{j1} X_{ij} \right)^2 \right\} \text{ subject to } \sum_{j=1}^{d} V_{j1}^2 = 1,$$

where $\bar{Z}_1 = \frac{1}{n} \sum_{i=1}^{n} Z_{i1}$ is the mean of Z_1. This mean is zero, as all columns of X are centered to zero.

Solving the problem above, we get the first *principal component loading vector* $V_1 \in \mathbb{R}^d$ and corresponding *score vector* $Z_1 \in \mathbb{R}^n$. The score vector provides a dimension-reduced representation of the original data.

After computing the first principal component loading vector V_1, we want to get the second principal component, that maximizes the variation uncorrelated to the first principal component Z_1. The procedure is the same as for the first principal component, but with a constraint that V_2 has to be orthogonal to V_1. We repeat these steps to get the first k principal component loading vectors and scores vectors, all of which are orthogonal. The whole method is the same as solving

$$\underset{V \in R^{d \times k}}{\text{argmax}} \ \text{tr}(V^T C_X V),$$

where $C_X = X^T X/n$ is the covariance matrix of X, and V is a $d \times k$ matrix with d as above and k the number of principal components. Each column of V, denoted V_j, is a d-dimensional vector that represents a principal component loading vector. These vectors are in fact the eigenvectors of C_X, and they maximize the variance captured in the projected data.

The principal component scores Z_j and loading vectors V_j can be used to explore and interpret the reduced-dimension data. The scores Z_j represent the projection of the original data onto the principal components, allowing for lower-dimensional visualizations that may identify patterns and/or clusters within the data. The loading vectors V_j reflect the contribution of each original variable to the principal components, providing insight into which features explain most of the variance captured by each principal component.

2.2 Minimizing the reconstruction error

Another justification of PCA is that it minimizes the reconstruction error (mean squared error) when projecting the dataset X to a lower dimensional space of dimension k. Here we want to find a matrix $V_{d \times k}$ whose columns form an orthonormal basis (i.e. $V^T V = I_k$, where I_k is an identity matrix of size k) for which the projection VV^T provides the best linear manifold approximation of the X. Formally this means solving

$$\underset{V \in R^{d \times k}}{\text{argmin}} \sum_{i=1}^{n} ||x_i - V_{d \times k} V_{d \times k}^T x_i||_2^2,$$

where each X_i is the ith row of the X and $V_{d\times k}$ is the first principal component loading vectors.

The matrix $V_{d\times k}$ can be computed from the eigen-decomposition of C_X

$$C_X = V\Lambda V^T,$$

where $V = (V_1, ..., V_k)$ are the k principal component loading vectors.

In practice, both of PCA's interpretations (maximizing variance captured and minimizing reconstruction error) are compelling, when our goal is simplifying complex datasets yet preserving their essential features. In practice, PCA analysis is widely-used, and its dimension-reduction of data improves cost and efficiency of analyses.

While PCA is effective in reducing dimensionality and identifying key patterns in cross-sectional datasets, it is not well-suited for data with temporal dependencies. PCA treats each data point independently and does not account for the sequential nature of time-series data, meaning it is not a good choice when we aim to capture the dynamics and temporal correlations inherent in such datasets (Brunton et al., 2016).

Addressing this limitation, Dynamic Mode Decomposition (DMD) is better-suited for for analyzing spatio-temporal data. Unlike PCA, DMD explicitly models temporal dynamics by decomposing data into modes that capture coherent structures evolving over time. The following Chapter describes the DMD algorithm and its variants.

Chapter 3

DMD METHODS

3.1 DMD

DMD is used to identify dominant spatial and temporal patterns within a dynamic system. It is particularly useful for studying complex systems that evolve over time, such as fluid flows, biological processes, or financial markets. It relies on the assumption that future data is a linear transformation of the past data. Therefore, the model can be written as

$$X^{(2)}_{\text{clean}} = AX^{(1)}_{\text{clean}},$$

where

$$\begin{aligned} X^{(1)}_{\text{clean}} &= \begin{bmatrix} x^{(1)}_{\text{clean}} & x^{(2)}_{\text{clean}} & \cdots & x^{(n)}_{\text{clean}} \end{bmatrix} \in \mathbf{R}^{d\times n}, \\ X^{(2)}_{\text{clean}} &= \begin{bmatrix} x^{(2)}_{\text{clean}} & x^{(3)}_{\text{clean}} & \cdots & x^{(n+1)}_{\text{clean}} \end{bmatrix} \in \mathbf{R}^{d\times n}, \end{aligned}$$

are noise-free datasets and where $x^{(i)}_{\text{clean}} = [x^{(i1)}_{\text{clean}}, x^{(i2)}_{\text{clean}}, \cdots, x^{(id)}_{\text{clean}}]^T$ for $i \geq 1$ is a snapshot at time i of the dynamical system that generated $X^{(1)}_{\text{clean}}$ and $X^{(2)}_{\text{clean}}$. $A \in \mathbf{R}^{d\times d}$ is the linear operator which maps $X^{(1)}_{\text{clean}}$ to $X^{(2)}_{\text{clean}}$. In this setting, in contrast to PCA, it is convenient to construct the data matrix such that each multivariate observation is represented by a column, not row, of $X^{(1)}_{\text{clean}}$ or $X^{(2)}_{\text{clean}} \in \mathbb{R}^{d\times n}$. Equivalently we can write

$$x^{(i)}_{\text{clean}} = Ax^{(i-1)}_{\text{clean}}, \tag{3.1}$$

where $i \geq 1$. In applied work clean data is usually not available, so we need to rely on noisy data to estimate A. Let X_1 and X_2 be the noisy version of $X^{(1)}_{\text{clean}}$ and $X^{(2)}_{\text{clean}}$ where the noise

is unknown. Exact DMD estimates A in a least-square manner where

$$\hat{A} = \underset{A \in R^{d \times d}}{\operatorname{argmin}} ||X_2 - AX_1||_2^2 = X_2 X_1^{\dagger}, \tag{3.2}$$

where $X_1^{\dagger}$ is the Moore–Penrose inverse of X_1. To find the Moore–Penrose inverse of X_1 we use the the singular value decomposition (SVD)

$$X_1 = U \Sigma V^*,$$

where both $U \in \mathbb{R}^{n \times n}$ and $V \in \mathbb{R}^{m \times m}$ are unitary. U contains the POD modes, which are a set of orthonormal spatial modes that capture the dominant patterns in X_1. $\Sigma \in \mathbb{R}^{n \times m}$ is a diagonal matrix where each diagonal value represents the contribution of each corresponding mode in U. The matrix A is hard to interpret as it represents the linear transformation of two dataset X_1 and X_2 that are collected at consecutive timepoints and it does not directly relate to any intuitive concepts. Additionally, A is often of high-dimension, and so its most important patterns are difficult to identify. Consequently, the interest is often in the decomposition of A into its eigenvalues and eigenvectors

$$A\Phi = \Phi\Lambda,$$

where the diagonal matrix $\Lambda \in \mathbb{R}^{d \times d}$ contains the eigenvalues of A and the matrix $\Phi \in \mathbb{R}^{d \times d}$ contains the eigenvalues of A, which are also the DMD modes. The eigenvalues provide information about the growth and oscillation of each mode over time, and eigenvectors represent the spatial patterns associated with these dynamics. Eigenvalues whose exponential is less than one (i.e. those inside the unit circle) correspond to decaying modes that decrease in amplitude over time. Those with magnitudes equal to one (on the unit circle) indicate stationary modes that do not change in amplitude over time. Those with magnitudes greater than one (outside the unit circle) correspond to growing modes which increase in amplitude over time. Complex eigenvalues with non-zero imaginary parts indicate oscillatory modes.

The real part determines whether the oscillation grows or decays, while the imaginary part indicates the frequency of the oscillation.

However, with $d > n$ the computation can be difficult. In this case, the computation of A requires solving an overdetermined system where the number of variables exceeds the number of observations. Similar to PCA analysis, we can solve this by estimating A through $\tilde{A}$, which is computed by projecting A onto the first r POD modes in U. More formally

$$\begin{aligned} AX_1 &= X_2 \\ \Rightarrow U^*AX_1 &= U^*X_2 \\ \Rightarrow U^*A(U\Sigma V^*) &= U^*X_2 \\ \Rightarrow U^*AU\Sigma V^* &= U^*X_2 \\ \Rightarrow U^*AU &= U^*X_2V\Sigma^{-1} \\ \Rightarrow \tilde{A} &= U_r^*X_2V_r\Sigma_r^{-1}. \end{aligned}$$

This eigenvalue problem for $\tilde{A}$ is solved by

$$\tilde{A}W = W\tilde{\Lambda},$$

where the diagonal matrix $\tilde{\Lambda}$ contains the DMD eigenvalues, which correspond to eigenvalues Λ of the high-dimensional matrix A. The columns of W are eigenvectors of $\tilde{A}$, which can be interpreted as a linear combination of the POD modes in U.

Given that, DMD modes can be constructed by

$$\Phi = UW.$$

Despite its known utility for analyzing spatio-temporal datasets, DMD is notably sensitive to noise, which can significantly decrease the accuracy of its outputs. This is because DMD estimates A in a least-square manner according to Equation (3.2). This is effectively a

regression problem, except that both the predictor (X_1) and the outcome (X_2) are noisy. In standard regression theory, noise in the outcome X_2 affects the accuracy of the model parameters but does not introduce bias into the estimate. However, noise in the predictor X_1 distorts the relationship between the predictor and the outcome and leads to a biased estimate of A's eigenvalues and eigenvectors.

3.2 Optimized DMD

The optimized DMD from Askham & Kutz (2018) is a modification of the standard DMD technique. It is designed to handle the effect from systematic noise by using the variable projection method (Golub & Pereyra, 1973), which fits an exponential model to the data. The variable projection method takes advantage of the unique structure of the exponential model fitting, allowing for the elimination of many uninterested variables (noise) from the optimization process. Additionally, under this setting, data snapshots no longer need to be taken at regular intervals, which is particularly useful when data are collected at unevenly spaced times (Askham & Kutz, 2018).

Let $X = [x_1, x_2, \cdots, x_{n+1}]$ where $x_i = [x_{i1}, x_{i2}, \cdots, x_{id}]^T$ $(i \geq 1)$ is snapshot at a time i of the dynamical system that generated X. Similarly to Equation (3.1), we want to find A such that

$$x_i = Ax_{i-1},$$

where $i = 1, 2, 3, ...$ Note that if the observations were equally spaced, we could rewrite our model as

$$x_i \approx A^i x_0,$$

But to account for having time steps of possibly different lengths, letting t_i denote the time of the ith observations, Optimized DMD assumes that

$$x_{t_i} \approx e^{At_i} x_{t_0} = S\Gamma^i S^\dagger x_{t_0}, \tag{3.3}$$

where e denotes the matrix exponential, $S \in \mathbb{R}^{n\times r}$, contains the eigenvectors of A as its columns, and $\Gamma \in \mathbb{R}^{r\times r}$ is a diagonal matrix with diagonal entries that are the exponential of the eigenvalues of A. r is the number of eigenvalues of interest. This can be rewritten as

$$X \approx \Phi(\lambda)B,$$

where $\Phi(\lambda) \in \mathbb{R}^{(m+1)\times r}$ with entries $\Phi(\lambda)_{ij} = \exp(\lambda_j t_i)$ and $B \in \mathbb{R}^{r\times n}$.

The optimized DMD seeks to solve the minimization problem

$$\min_{\lambda\in\mathbb{R}^k, B\in\mathbf{R}^{l\times n}} \|X - \Phi(\lambda)B\|_F. \tag{3.4}$$

To solve this problem, it uses the variable projection method, which involves separating the optimization over λ and B.

For a fixed λ, the problem reduces to the linear least squares problem

$$\min_{B\in R^{l\times n}} \|X - \Phi(\lambda)B\|_F. \tag{3.5}$$

and the optimal B for a given λ can be found using the pseudo-inverse

$$B(\lambda) = \Phi(\lambda)^\dagger X. \tag{3.6}$$

Substituting $B(\lambda)$ back into the original problem, we obtain

$$\min_{\lambda\in R^k} \|X - \Phi(\lambda)\Phi(\lambda)^\dagger X\|_F. \tag{3.7}$$

This problem can be solved using iterative optimization techniques such as gradient descent, Gauss-Newton, or Levenberg-Marquardt algorithms. The eigenvalues estimated through the exact DMD method are used as the initial λ for the optimization mechanism.

Once the optimal λ^* and B^* are found, the optimized DMD eigenvalues λ_i and eigenmodes

ϕ_i are defined as:

$$\begin{aligned} \lambda_i &= \lambda_i^*, \\ \phi_i &= \frac{1}{\|B^*(:,i)\|_2} B^*(:,i), \end{aligned}$$

where $B^*(:,i)$ is the i-th column of B^*.

Optimized DMD rephrases the DMD into a exponential model fitting problem as presented in Equation (3.3) and all snapshots are processed collectively throughout the optimization—see Equations (3.5), (3.6), and (3.7). This setup allows Optimized DMD to smooth out the noise in optimization and thus has a more robust and accurate estimation of eigenvalues and eigenvectors.

3.3 Modified Optimized DMD

Here we introduce our modified version of optimized DMD. Optimized DMD uses the eigenvalues estimated through the exact DMD approach as the initial α for the optimization. In this modified version, a de-biased initial alpha estimate is used. Let $X_{\text{clean}} = [x_{\text{clean}}^{(1)}, x_{\text{clean}}^{(2}, ..., x_{\text{clean}}^{(n+1)}]$ be the noise-free data, $E \in \mathbf{R}^{d\times(n+1)}$ be the error independent of X and $\Sigma_E \in \mathbf{R}^{d\times d}$ be the known covariance of the error introduced to the data. In that case, the observed X is

$$X = X_{\text{clean}} + E.$$

Assume we have an estimate of Σ_E, that we call $\hat{\Sigma}_E$, and define the $X_{\text{modified}} \in \mathbf{R}^{d\times(n+1)}$ as

$$X_{\text{modified}} = X\hat{\Sigma}_E^{-1/2} = (X_{\text{clean}} + E)\hat{\Sigma}_E^{-1/2} = X_{\text{clean}}\hat{\Sigma}_E^{-1/2} + E\hat{\Sigma}_E^{-1/2},$$

where $\hat{\Sigma}_E^{-1/2} \in \mathbf{R}^{d\times d}$ is the inverse of the matrix square root of $\hat{\Sigma}_E$. Given that the error term is independent of X, we have

$$\text{Cov}(X_{\text{modified}}) \approx (\Sigma_E^{-1/2})^T \text{Cov}(X_{\text{clean}})\Sigma_E^{-1/2} + I_{d\times d}.$$

As adding a diagonal matrix does not affect the computation of eigenvectors, the modified DMD modes Φ_{modified} we got by applying the Exact DMD to the X_{modified} are consistent with the DMD modes computed based on clean data X_{clean}. As a result, we can use Phi_{modified} as a subspace onto which the input data can be projected in order to reduce its dimension and to help Optimized DMD focus on the most dominant modes.

In our application, the covariance of the error term ϵ is unknown, but it can be estimated by using our data's replicate measurements. Specifically, suppose we have R replicates of the $n \times m$ data matrix X. Let $X^{(r)}$ represent the r-th replicate, where $r = 1, 2, \ldots, R$. Calculating the mean of the replicates for each element in the matrix, we define

$$\bar{X}_{ij} = \frac{1}{R} \sum_{r=1}^{R} X_{ij}^{(r)},$$

for each element (i, j) in the matrix, where $i = 1, 2, \ldots, n$ and $j = 1, 2, \ldots, m$.

Computing the residuals for each element in each replicate, we obtain

$$E_{ij}^{(r)} = X_{ij}^{(r)} - \bar{X}_{ij}.$$

Stacking the residual matrices $E^{(r)}$ into a single matrix E in which each column represents the residuals from one replicate, we obtain an $(n \cdot m) \times R$ matrix

$$E = \begin{pmatrix} \vdots & \vdots & \vdots & \\ \text{vec}(E^{(1)}) & \text{vec}(E^{(2)}) & \cdots & \text{vec}(E^{(R)}) \\ \vdots & \vdots & \vdots & \end{pmatrix}, \tag{3.8}$$

where $\text{vec}(E^{(r)})$ denotes the vectorization of the matrix $E^{(r)}$. The lets us denote an estimate of the covariance matrix of the error term as simply

$$\hat{\Sigma_E} = \frac{1}{R-1} E E^T.$$

Chapter 4

SIMULATION

4.1 Simulation Setup

In this section, we compare the performance of the different DMD algorithms on a simple example with additive noise. Performance was assessed by comparing the eigenvalues computed using exact DMD, optimized DMD, and modified optimized DMD with the true eigenvalues, under 6 simulation settings. For each setting, 1000 replications were run for each method.

The data used in this example was generated by constructing

$$\begin{aligned} x_{\text{clean}}^{t_i} &= A x_{\text{clean}}^{t_{i-1}}, \\ A\Phi &= \Phi\Lambda, \end{aligned}$$

where $x_{\text{clean}}^{t_i} \in \mathbb{R}^d$ is the vector of observations at time $t_i \in (0, 200)$. Linear operator $A \in \mathbb{R}^{d\times d}$ describes the dynamics of the data. The eigenvectors of A are the DMD modes Φ and the eigenvalues of A are the leading diagonal elements in the diagonal matrix Λ. For the case of MEG data, each column of Φ corresponds to a spatial pattern of all magnetometer channels, as presented in Figure 1.1, that captures the neural activity, and the eigenvalues in Λ capture the temporal dynamics associated with these patterns. This means that while Φ reveals how neural activity is distributed across different channels, Λ provides insight into how these patterns evolve over time. $x_{\text{clean}}^{t_0} \in \mathbb{R}^d$ is a pre-specified vector that indicates the initial values of the d variables at time 0. We generate the full clean data X_{clean} based on these initial values. We don't expect the initial values to impact the DMD modes, but the sensitivity with respect to this parameter may require further investigation. To simulate the actual observations, we add noise to the X_{clean} that mimics the noise introduced during the

MEG data collection

$$X = X_{\text{clean}} + E,$$

where $E \sim MVN(0,\ \Sigma_E)$, with positive definite $\Sigma_E \in \mathbb{R}^{d\times d}$. We set Σ_E to represent six different settings:

1. Low and uncorrelated noise

$$\Sigma_{\text{E(low, uncorrelated)}} = \begin{bmatrix} \sigma_1^2 & 0 & 0 \\ 0 & \sigma_2^2 & 0 \\ 0 & 0 & \sigma_3^2 \end{bmatrix},$$

   where $\sigma_1 = 0.03$, $\sigma_2 = 0.02$, and $\sigma_3 = 0.05$.

2. Medium and uncorrelated noise

$$\Sigma_{\text{E(medium, uncorrelated)}} = 10\Sigma_{\text{E(low, uncorrelated)}}.$$

3. High and uncorrelated noise

$$\Sigma_{\text{E(high, uncorrelated)}} = 100\Sigma_{\text{E(low, uncorrelated)}}.$$

4. Low and correlated noise:

$$\Sigma_{\text{E(low, correlated)}} = \begin{bmatrix} \sigma_1^2 & \sigma_1\sigma_2\rho_{12} & \sigma_1\sigma_3\rho_{13} \\ & \sigma_2^2 & \sigma_2\sigma_3\rho_{23} \\ & & \sigma_3^2 \end{bmatrix},$$

   in which the σ_i^2 terms are identical to those in simulation setting 1, $\rho_{12} = 0.33$, $\rho_{13} = 0.04$, and $\rho_{23} = 0.1$ represent the correlation between the corresponding columns.

5. Medium and correlated noise

$$\Sigma_{\text{E(medium, correlated)}} = 10\Sigma_{\text{E(low, correlated)}}.$$

6. High and correlated noise

$$\Sigma_{\text{E(high, correlated)}} = 100\Sigma_{\text{E(low, correlated)}}.$$

The effect of noise on the first variable across different noise settings is illustrated in Figure 4.1. The effect of noise on the second and third variables are attached in the Appendix A.1 and A.2.

4.2 Simulation Results and Discussion

The performance of the DMD algorithms was assessed by examining the real and imaginary parts of the eigenvalues they return under different noise conditions. The aims were to evaluate how well these algorithms handle additive noise, and to compare their effectiveness in terms of estimation error and variance. The results are consistent among all 6 simulation settings, so in the following subsections, we only focus on presenting and interpreting the results from the medium uncorrelated noise setting and medium correlated noise setting. The outputs of other simulation settings are given in the Appendix tables B.1 to B.8 and Appendix figures B.1 to B.8.

4.2.1 Medium and Uncorrelated Noise

The violin plots in Figure 4.2 (a), (c), and (e) demonstrate that the Optimized and Modified Optimized DMD methods provide notably more accurate estimates for the eigenvalue real part compared to the Exact DMD across all eigenvalues and replications. Additionally, plots (b), (d), and (f) show that the estimates from the Modified Optimized DMD are more concentrated around the true eigenvalue real part. As shown in Table 4.1, the Modified

Optimized DMD consistently produced the lowest average estimation error, empirical standard deviation, and mean squared error across all three eigenvalues real part estimation. For the first eigenvalue, the Modified Optimized DMD achieves an average estimation error of 1.59×10^{-4}, which is lower than the Optimized DMD's error of 2.29×10^{-4}. Additionally, the empirical standard deviation (SD) and mean squared error (MSE) for the Modified Optimized DMD are 7.07×10^{-4} and 5.25×10^{-7}, respectively, compared to 9.59×10^{-4} and 9.72×10^{-7} for the Optimized DMD. These improvements are also observed for the second and third eigenvalues. The differences in eigenvalue real part estimates from Optimized DMD and Modified Optimized DMD is 2.30, 2.45, and 3.00 times larger than the corresponding *Monte Carlo errors* (Emprical SD/$\sqrt{1000}$) for the three eigenvalues, which indicates that the difference between two methods are well beyond what we might expect by chance alone.

Similar results have been found for eigenvalues imaginary part. The violin plots in Figure 4.2 (a), (c), and (e) demonstrate that the Optimized and Modified Optimized DMD methods provide notably more accurate estimates for the eigenvalue imaginary part compared to the Exact DMD across all eigenvalues and replications. Additionally, plots (b), (d), and (f) show that the estimates from the Modified Optimized DMD are more concentrated around the true eigenvalue imaginary part. As shown in Table 4.2, the Modified Optimized DMD consistently produced the lowest average estimation error, empirical standard deviation, and mean squared error across all three eigenvalues imaginary part estimation. For the first eigenvalue, the Modified Optimized DMD achieves an average estimation error of 8.54×10^{-4}, which is lower than the Optimized DMD's error of 1.37×10^{-3}. Additionally, the empirical standard deviation (SD) and mean squared error (MSE) for the Modified Optimized DMD are 1.46×10^{-3} and 2.86×10^{-6}, respectively, compared to 2.22×10^{-3} and 6.79×10^{-6} for the Optimized DMD. These improvements are also observed for the second and third eigenvalues. The differences in eigenvalue imaginary part estimates from Optimized DMD and Modified Optimized DMD is 7.35, 7.22, and 2.50 times larger than the corresponding Monte Carlo errors (Emprical SD/$\sqrt{1000}$) for the three eigenvalues, which indicates that the difference between two methods are well beyond what we might expect by chance alone.

Thus, for the eigenvalue real and imaginary part under medium uncorrelated noise condition, both Optimized DMD and Modified Optimized DMD produce substantially more accurate estimates than the Exact DMD. Modified Optimized DMD further surpasses the Optimized DMD by offering lower average estimation error, empirical standard deviation, and mean squared error, as well as a more concentrated distribution of estimates around the actual eigenvalue.

Variable	**Method**	**Bias**	**Empirical SD**	**MSE**
First	Exact	-5.41×10^{-2}	1.09×10^{-2}	3.05×10^{-3}
	Optimized	2.29×10^{-4}	9.59×10^{-4}	9.72×10^{-7}
	Modified	1.59×10^{-4}	7.07×10^{-4}	5.25×10^{-7}
Second	Exact	-4.64×10^{-2}	4.80×10^{-3}	2.18×10^{-3}
	Optimized	2.35×10^{-4}	9.59×10^{-4}	9.74×10^{-7}
	Modified	1.60×10^{-4}	7.09×10^{-4}	5.28×10^{-7}
Third	Exact	-6.51×10^{-2}	7.92×10^{-3}	4.30×10^{-3}
	Optimized	-1.42×10^{-4}	1.04×10^{-3}	1.10×10^{-6}
	Modified	-4.34×10^{-5}	6.92×10^{-4}	4.81×10^{-7}

Table 4.1: Bias (Averaged Estimation Error), empirical standard deviation (SD), and mean squared error (MSE) for the real eigenvalues under medium uncorrelated noise settings across different DMD algorithms.

4.2.2 Medium and Correlated Noise

The violin plots in Figure 4.4 (a), (c), and (e) demonstrate that the Optimized and Modified Optimized DMD methods provide more accurate estimates for the eigenvalues' real part compared to the Exact DMD across all eigenvalues and replications. Additionally, plots (b), (d), and (f) show that the estimates from the Modified Optimized DMD are slightly more concentrated around the true eigenvalue real part. As shown in Table 4.3, the Modified Optimized DMD consistently produced the lowest average estimation error, empirical standard deviation, and mean squared error across all three eigenvalues real part estimation. For the first eigenvalue, the Modified Optimized DMD achieves an average estimation error of

Variable	Method	Bias	Empirical SD	MSE
First	Exact	1.22×10^{-2}	4.54×10^{-3}	1.70×10^{-4}
	Optimized	1.37×10^{-3}	2.22×10^{-3}	6.79×10^{-6}
	Modified	8.54×10^{-4}	1.46×10^{-3}	2.86×10^{-6}
Second	Exact	-7.51×10^{-2}	3.90×10^{-2}	7.16×10^{-3}
	Optimized	-1.35×10^{-3}	2.18×10^{-3}	6.59×10^{-6}
	Modified	-8.52×10^{-4}	1.45×10^{-3}	2.83×10^{-6}
Third	Exact	6.29×10^{-2}	3.82×10^{-2}	5.41×10^{-3}
	Optimized	-1.99×10^{-5}	2.22×10^{-4}	4.96×10^{-8}
	Modified	-2.40×10^{-6}	1.38×10^{-4}	1.90×10^{-8}

Table 4.2: Bias (Averaged Estimation Error), empirical standard deviation (SD), and mean squared error (MSE) for the imaginary eigenvalues under medium uncorrelated noise settings across different DMD algorithms.

1.42×10^{-4}, which is lower than the Optimized DMD's error of 2.33×10^{-4}. Additionally, the empirical standard deviation (SD) and mean squared error (MSE) for the Modified Optimized DMD are 6.68×10^{-4} and 4.66×10^{-7}, respectively, compared to 1.05×10^{-3} and 1.16×10^{-6} for the Optimized DMD. These improvements are also observed for the second and third eigenvalues. The differences in eigenvalue real part estimates from Optimized DMD and Modified Optimized DMD is 2.74, 2.69, and 4.22 times larger than the corresponding Monte Carlo errors for the three eigenvalues, which indicates that the differences between the two methods are unlikely to be due to chance. The violin plots in Figure 4.5 indicate that all three methods have high bias for the eigenvalue imaginary part estimation.

Similar results have been found for eigenvalues imaginary part. The violin plots in Figure 4.3 (a), (c), and (e) demonstrate that the Optimized and Modified Optimized DMD methods provide notably more accurate estimates for the eigenvalue imaginary part compared to the Exact DMD across all eigenvalues and replications. Additionally, plots (b), (d), and (f) show that the estimates from the Modified Optimized DMD are more concentrated around the true eigenvalue imaginary part. As shown in Table 4.4, the Modified Optimized DMD consistently produced the lowest average estimation error, empirical standard devi-

ation, and mean squared error across all three eigenvalues imaginary part estimation. For the first eigenvalue, the Modified Optimized DMD achieves an average estimation error of 7.43×10^{-4}, which is lower than the Optimized DMD's error of 1.33×10^{-3}. Additionally, the empirical standard deviation (SD) and mean squared error (MSE) for the Modified Optimized DMD are 1.23×10^{-3} and 2.06×10^{-6}, respectively, compared to 2.04×10^{-3} and 5.94×10^{-6} for the Optimized DMD. These improvements are also observed for the second and third eigenvalues. The differences in eigenvalue imaginary part estimates from Optimized DMD and Modified Optimized DMD is 9.08, 9.06, and1.39 times larger than the corresponding Monte Carlo errors (Emprical SD/$\sqrt{1000}$) for the three eigenvalues, which indicates that the difference between two methods are well beyond what we might expect by chance alone.

Thus, for the eigenvalue real and imaginary part under medium correlated noise condition, both Optimized DMD and Modified Optimized DMD produce substantially more accurate estimates than the Exact DMD. Modified Optimized DMD further surpasses the Optimized DMD by offering lower average estimation error, empirical standard deviation, and mean squared error, as well as a more concentrated distribution of estimates around the actual eigenvalue.

4.2.3 Discussion

The outputs from other simulation settings are similar to the two cases discussed above. In summary, Optimized DMD and Modified Optimized DMD did better in estimating the both real and imaginary part of the eigenvalues from noisy data. Furthermore, Modified Optimized DMD showed an improvement over the Optimized DMD, by achieving not only smaller bias, empirical standard deviation, and mean square error across all simulation settings. Despite that Modified Optimized DMD overall produced more accurate eigenvalue estimates across all setting, the improvement in estimation to the corresponding Monte Carlo error ratio (difference between Optimized DMD estimate and Modified Optimized DMD estimate/Monte Carlo error) is lower in the other four noise setting outputs. In the low and uncorrelated noise setting, the ratio (0.15, 0.21, 0.92) for eigenvalue real part estimate and is

(2.91, 2.75, 2.06) for eigenvalue imaginary part estimate; In the high and uncorrelated noise setting, the ratio is (0.04, 0.25, 2.16) for eigenvalue real part estimate and is (0.84, 2.47, 2.91) for eigenvalue imaginary part estimate; In the low and correlated noise setting, the ratio is (2.18, 2.31, 1.52) for eigenvalue real part estimate and is (4.20, 4.06, 1.95) for eigenvalue imaginary part estimate; In the high and correlated noise setting, the ratio is (0.80, 1.23, 2.81) for eigenvalue real part estimate and is (3.31, 3.55, 1.76) for eigenvalue imaginary part estimate. This indicates that the difference between estimation from Optimized DMD and Modified Optimized DMD in these cases is relatively minor compared to those in the medium uncorrelated and medium correlated noise setting.

Variable	**Method**	**Bias**	**Empirical SD**	**MSE**
First	Exact	-5.41×10^{-2}	1.11×10^{-2}	3.05×10^{-3}
	Optimized	2.33×10^{-4}	1.05×10^{-3}	1.16×10^{-6}
	Modified	1.42×10^{-4}	6.68×10^{-4}	4.66×10^{-7}
Second	Exact	-4.36×10^{-2}	4.58×10^{-3}	1.92×10^{-3}
	Optimized	2.36×10^{-4}	1.05×10^{-3}	1.16×10^{-6}
	Modified	1.46×10^{-4}	6.73×10^{-4}	4.74×10^{-7}
Third	Exact	-6.91×10^{-2}	1.61×10^{-2}	5.03×10^{-3}
	Optimized	-1.37×10^{-4}	9.37×10^{-4}	8.96×10^{-7}
	Modified	-1.25×10^{-5}	5.96×10^{-4}	3.55×10^{-7}

Table 4.3: Bias (Averaged Estimation Error), empirical standard deviation (SD), and mean squared error (MSE) for the real eigenvalues under medium correlated noise settings across different DMD algorithms.

Variable	Method	Bias	Empirical SD	MSE
First	Exact	1.69×10^{-2}	5.09×10^{-3}	3.13×10^{-4}
	Optimized	1.33×10^{-3}	2.04×10^{-3}	5.94×10^{-6}
	Modified	7.43×10^{-4}	1.23×10^{-3}	2.06×10^{-6}
Second	Exact	-9.14×10^{-2}	2.39×10^{-2}	8.92×10^{-3}
	Optimized	-1.33×10^{-3}	2.03×10^{-3}	5.90×10^{-6}
	Modified	-7.43×10^{-4}	1.25×10^{-3}	2.10×10^{-6}
Third	Exact	7.44×10^{-2}	2.33×10^{-2}	6.08×10^{-3}
	Optimized	-3.29×10^{-6}	7.91×10^{-5}	6.26×10^{-9}
	Modified	1.96×10^{-7}	1.42×10^{-4}	2.00×10^{-8}

Table 4.4: Bias (Averaged Estimation Error), empirical standard deviation (SD), and mean squared error (MSE) for the imaginary eigenvalues under medium correlated noise settings across different DMD algorithms.

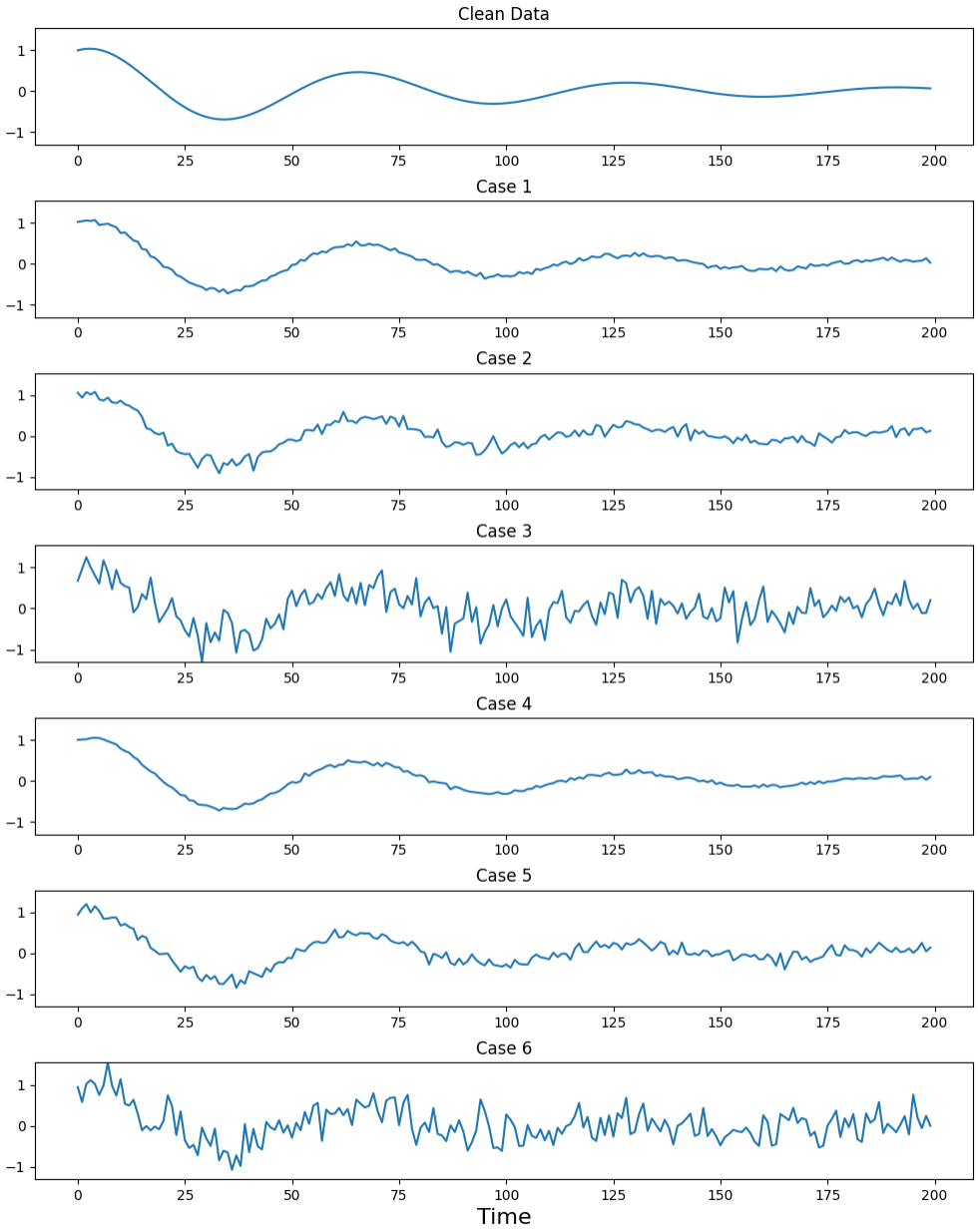

Figure 4.1: Effect of different noise settings on the first variable over time. The first plot shows the clean data without any noise. Subsequent plots illustrate the impact of low, medium, and high levels of uncorrelated noise (Cases 1, 2, and 3), followed by the impact of low, medium, and high levels of correlated noise (Cases 4, 5, and 6).

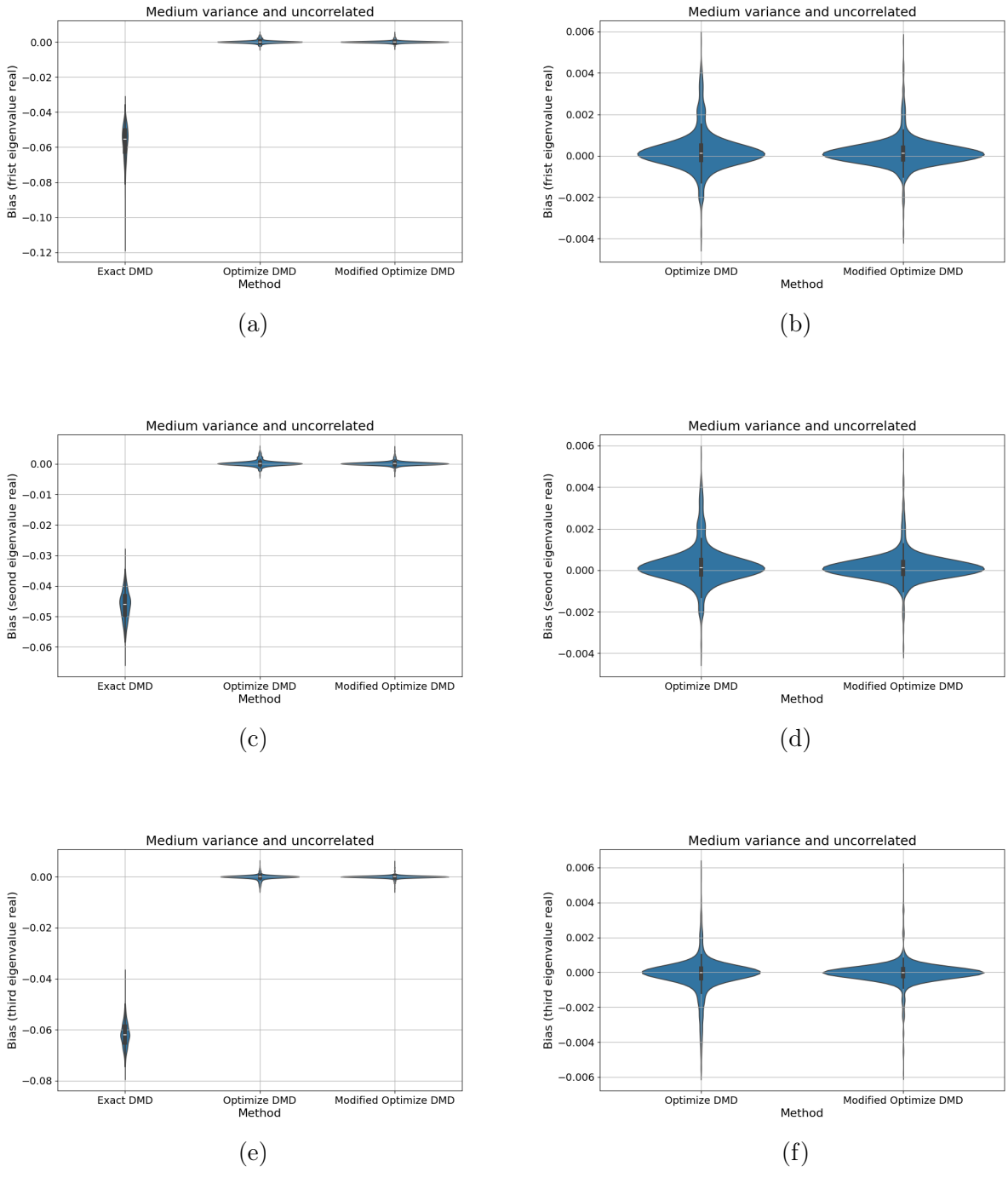

Figure 4.2: Estimation error quantification for estimate of the eigenvalues' real parts under medium variance and uncorrelated simulation setting. The violin plots illustrate the estimation error of the identified eigenvalues for Exact DMD, Optimize DMD, and Modified DMD methods. (a) and (b) show the estimation error distribution for the estimates of the real part of the first eigenvalue, (c) and (d) show the estimation error distribution for the estimated real part of the second eigenvalue, and (e) and (f) show the error distribution for the estimate of the real part of the third eigenvalue.

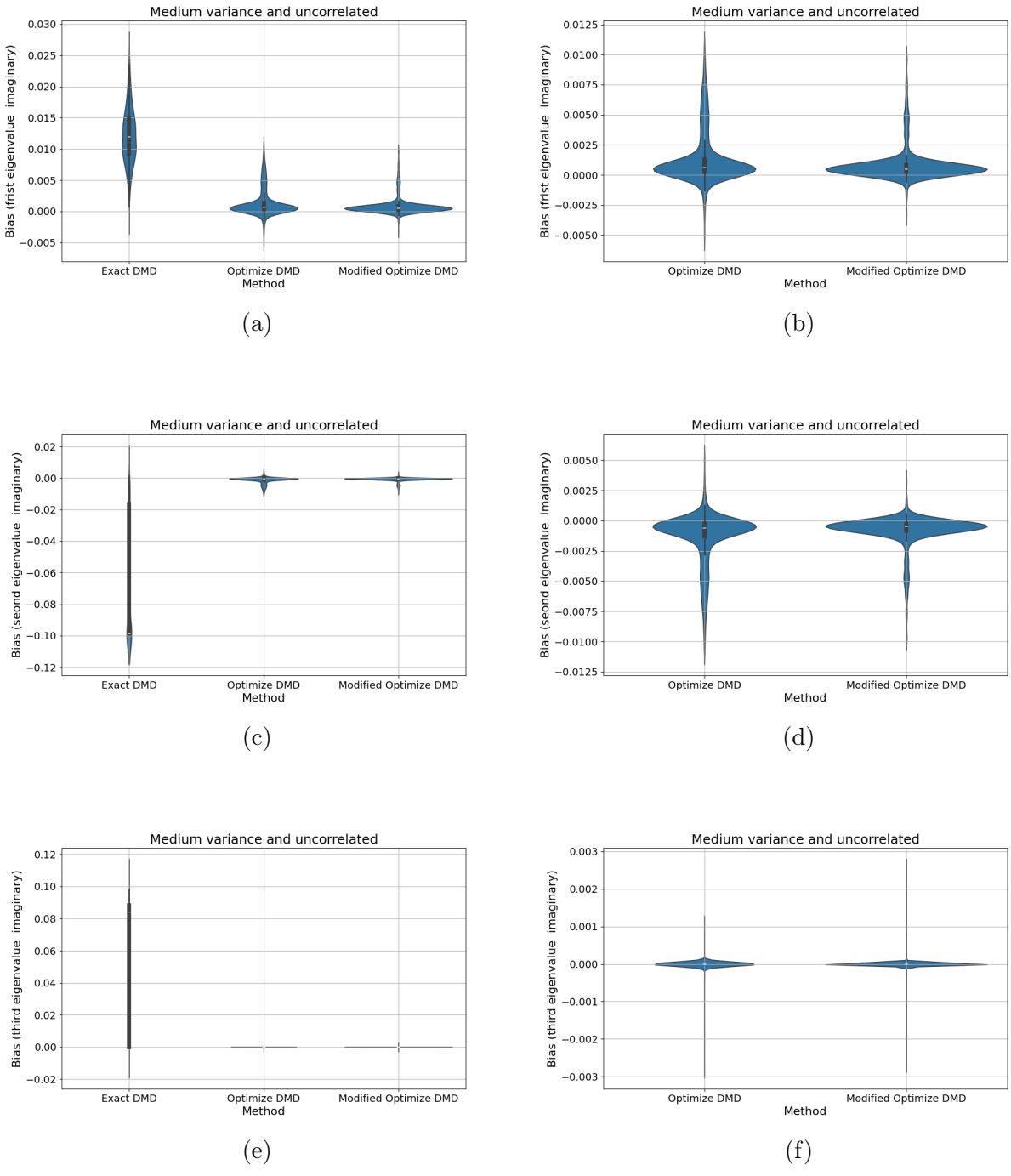

Figure 4.3: Estimation error quantification for estimate of the eigenvalues' imaginary parts under medium variance and uncorrelated simulation setting. The violin plots illustrate the estimation error of the identified eigenvalues for Exact DMD, Optimize DMD, and Modified DMD methods. (a) and (b) show the estimation error distribution for the estimates of the real part of the first eigenvalue, (c) and (d) show the estimation error distribution for the estimated real part of the second eigenvalue, and (e) and (f) show the error distribution for the estimate of the real part of the third eigenvalue.

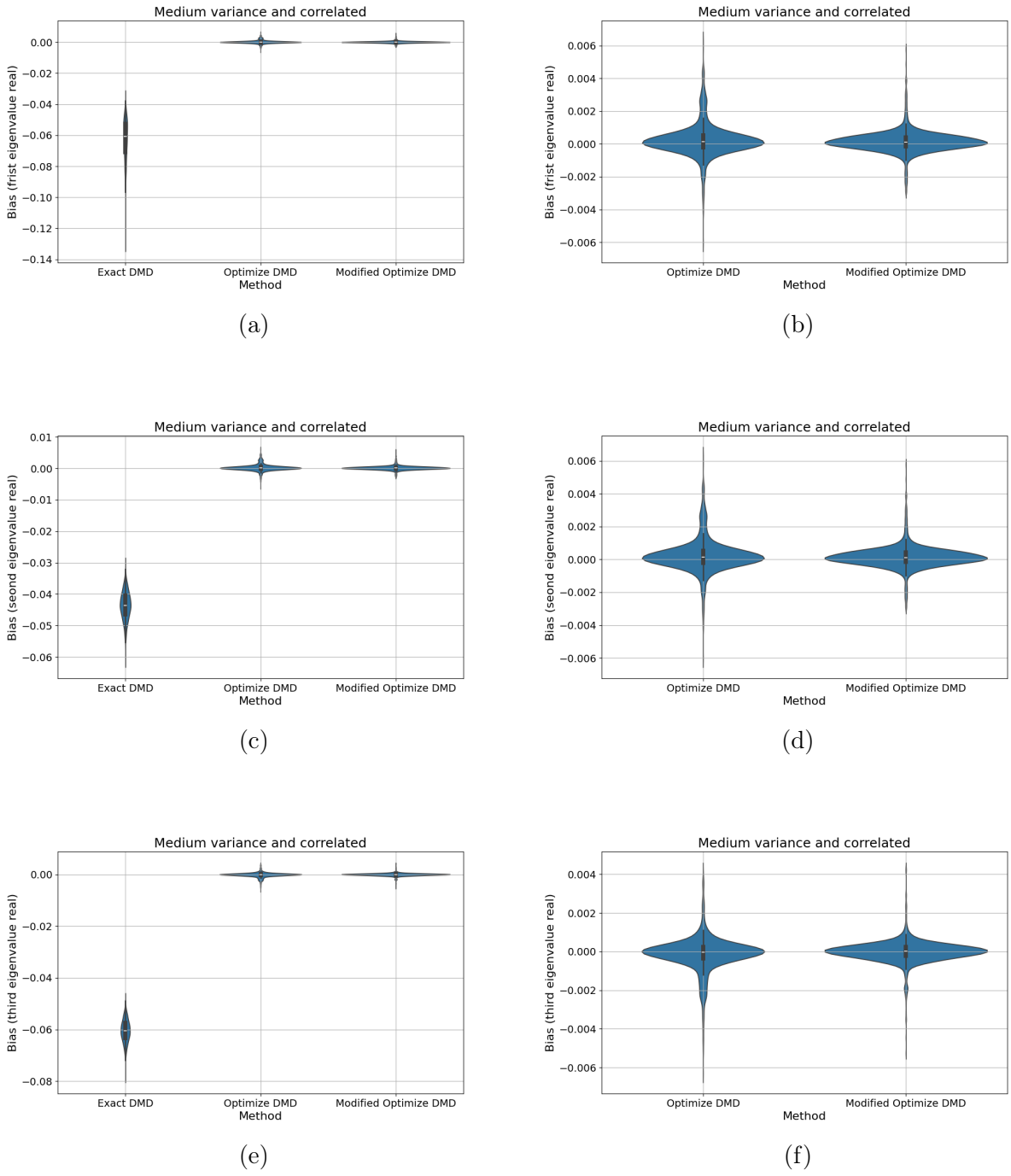

Figure 4.4: Estimation error quantification for estimate of the eigenvalues' real parts under medium variance and correlated simulation setting. The violin plots illustrate the estimation error of the identified eigenvalues for Exact DMD, Optimize DMD, and Modified DMD methods. (a) and (b) show the estimation error distribution for the estimates of the real part of the first eigenvalue, (c) and (d) show the estimation error distribution for the estimated real part of the second eigenvalue, and (e) and (f) show the error distribution for the estimate of the real part of the third eigenvalue.

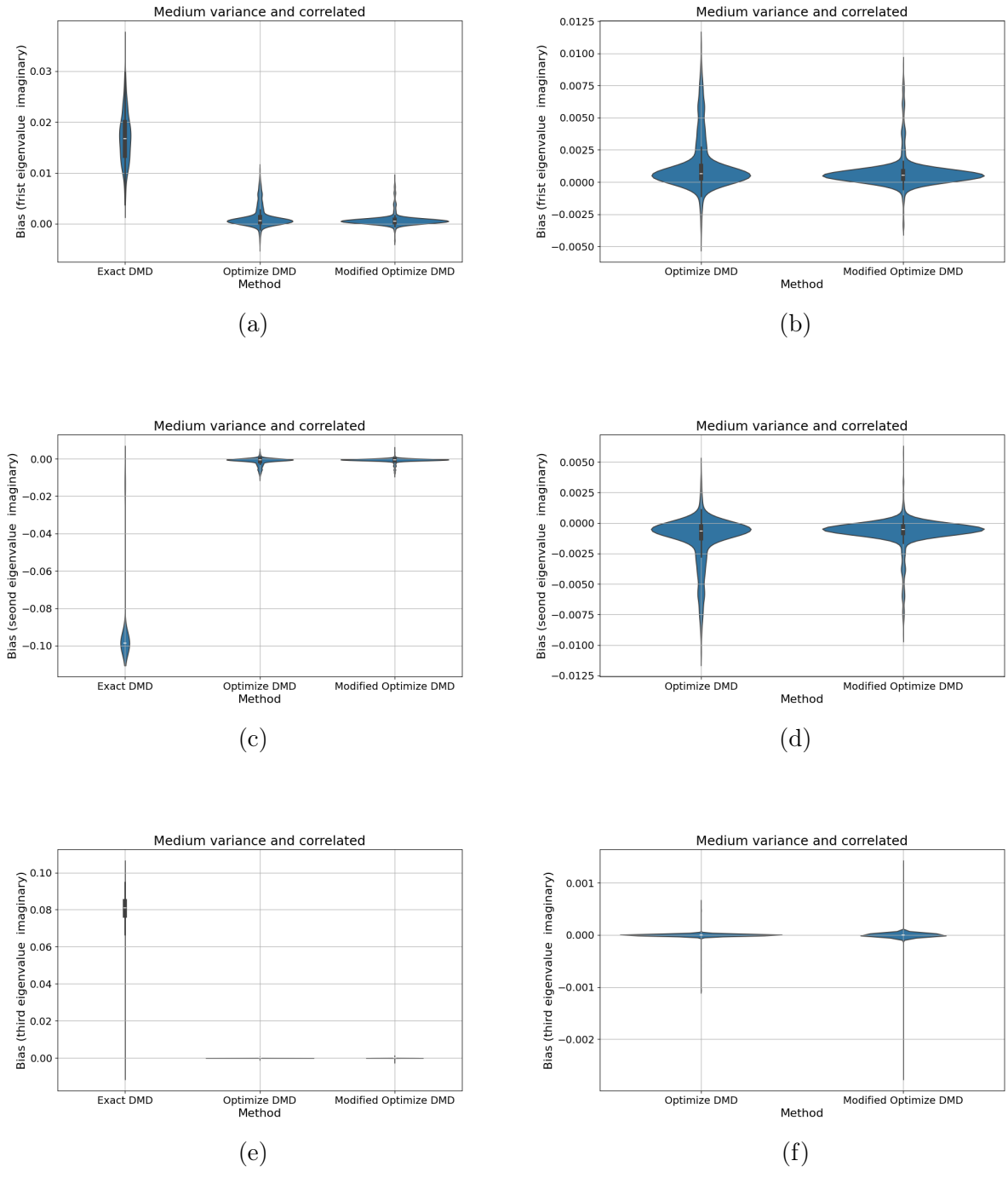

Figure 4.5: Estimation error quantification for estimate of the eigenvalues' imaginary parts under medium variance and correlated simulation setting. The violin plots illustrate the estimation error of the identified eigenvalues for Exact DMD, Optimize DMD, and Modified DMD methods. (a) and (b) show the estimation error distribution for the estimates of the real part of the first eigenvalue, (c) and (d) show the estimation error distribution for the estimated real part of the second eigenvalue, and (e) and (f) show the error distribution for the estimate of the real part of the third eigenvalue.

Chapter 5

MEG DATA

The data comes from an experiment in which a 17-year-old male subject was shown an emoji image while his brain activity was recorded using MEG. The data captured the magnetic fields generated by neural activity in the brain over a period of 0.748 seconds after the image appeared, with 188 snapshots being taken at regular intervals. Each snapshot represents the magnetic field strength measured by the 102 magnetometer channels at a specific moment in time. This procedure was repeated 140 times, resulting in 140 replicates of the subject's neural response to variationsof the emoji stimuli. It comprises time-series data from 102 magnetometer channels, capturing the magnetic field strength (fT) as a function of time (s). Figures 1.1 and 5.1 illustrate the detailed time series data for the first event, which in the following section we use to compare the performance of different DMD methods.

5.1 Application to MEG data

Exact DMD, Optimized DMD, and Modified Optimized DMD algorithms were applied to the MEG data. The covariance of the error term ϵ required for the Modified Optimized DMD was estimated using all 140 MEG replicates. The first three eigenvalues and corresponding eigenvectors were reported.

As shown in Table 5.1, the Exact DMD produced eigenvalues that are close to the unit circle in the complex plane, indicating nearly stationary dynamics with eigenvalues of $1.00 + 0.j$, $0.98 + 0.02j$, and $0.98 - 0.02j$. In contrast, the Optimized DMD resulted in complex eigenvalues, $0.38 \pm 1.46j$ and $2.42 + 9.75 \times 10^{-27}j$, suggesting a dynamic behavior with more pronounced oscillatory components. The Modified Optimized DMD, on the other hand, produced eigenvalues that diverged notably from both Exact and Optimized DMD, with

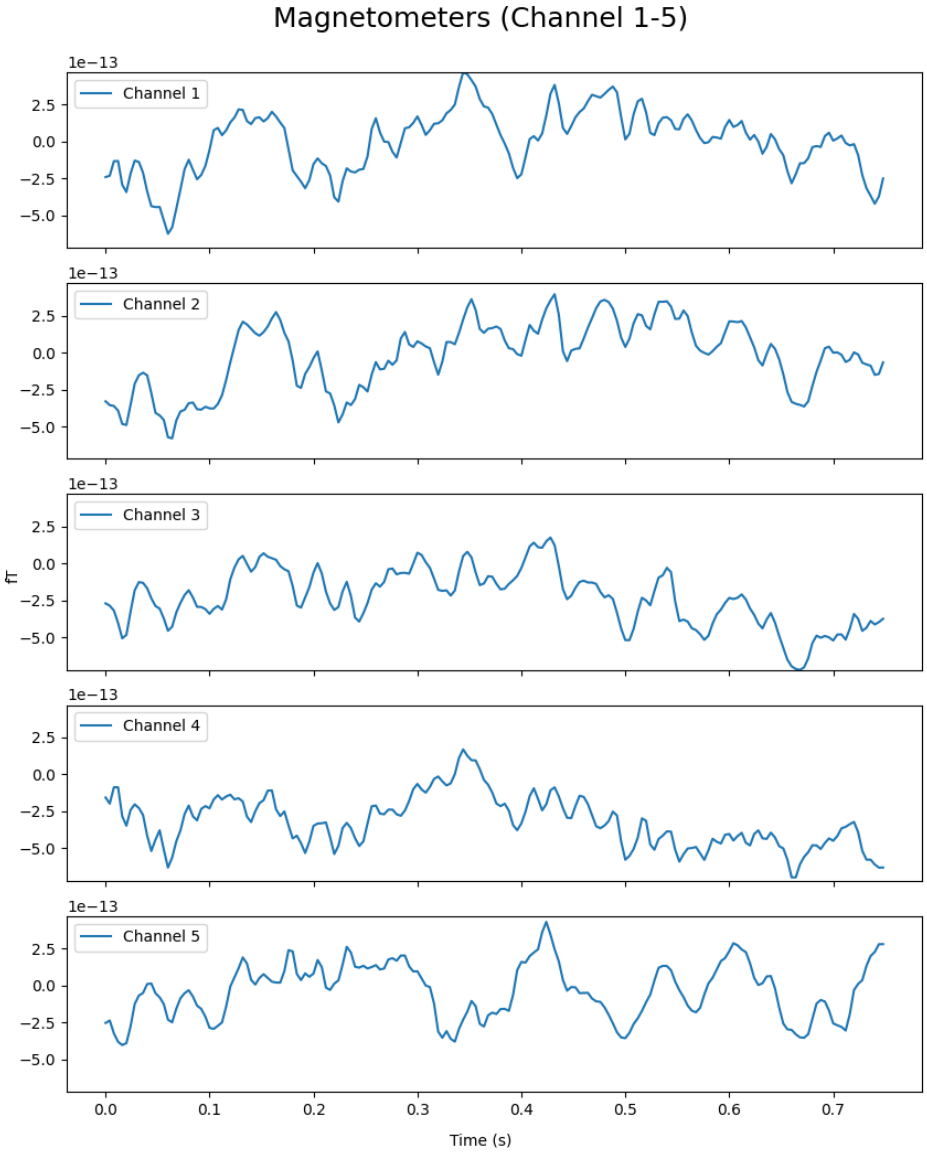

Figure 5.1: Time series data from the first five magnetometer channels in the MEG dataset. The plots display the magnetic field strength (fT) as a function of time (s) for channels 1 through 5. The data reveal fluctuations in the magnetic field, which correspond to neuronal activity detected by the magnetometers. This detailed view of individual channels shows a closer view of the signal characteristics at specific sensor locations.

values of $-1.12 + 1.16j$, $-1.16 - 1.15j$, and $2.27 - 4.07 \times 10^{-4}j$.

The analysis of the real part of the corresponding eigenvectors is visualized in Figure

5.2. The Exact DMD eigenvectors exhibit relatively smooth spatial patterns, with broad regions of positive and negative amplitudes. In contrast, the Optimized DMD provides more complex spatial patterns. The Modified Optimized DMD produces eigenvectors with reduced amplitude, but the spatial patterns are more distinct and exhibit sharper transitions between positive and negative regions. These are qualitatively similar to those produced by Optimized DMD.

Eigen Value	**Exact DMD**	**Optimized DMD**	**Modified Opt DMD**
First	$1.00 + 0.j$	$0.38 + 1.46j$	$-1.12 + 1.16j$
Second	$0.98 + 0.02j$	$0.38 - 1.46j$	$-1.16 - 1.15j$
Third	$0.98 - 0.02j$	$2.42 + 9.75 \times 10^{-27}j$	$2.27 - 4.07 \times 10^{-4}j$

Table 5.1: Comparison of the first three eigenvalues calculated by Exact DMD, Optimized DMD, and Modified Optimized DMD.

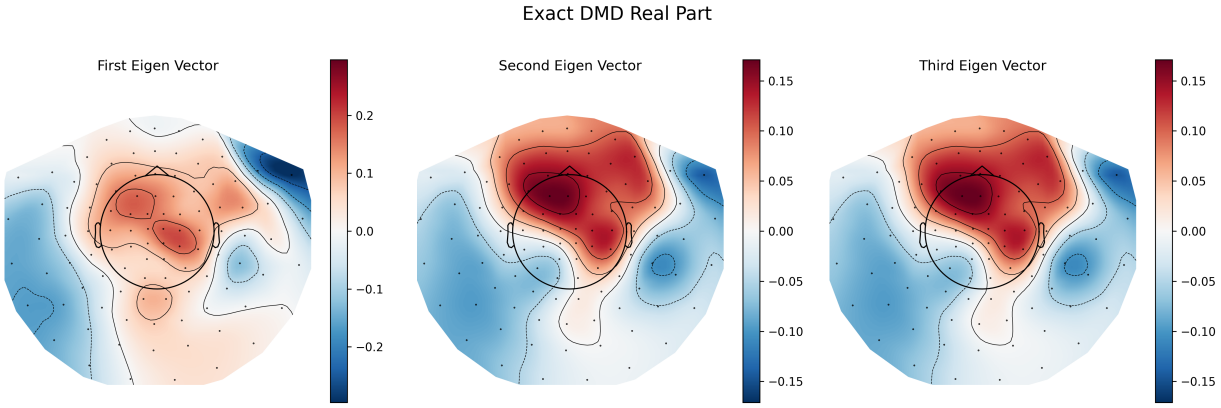

(a)

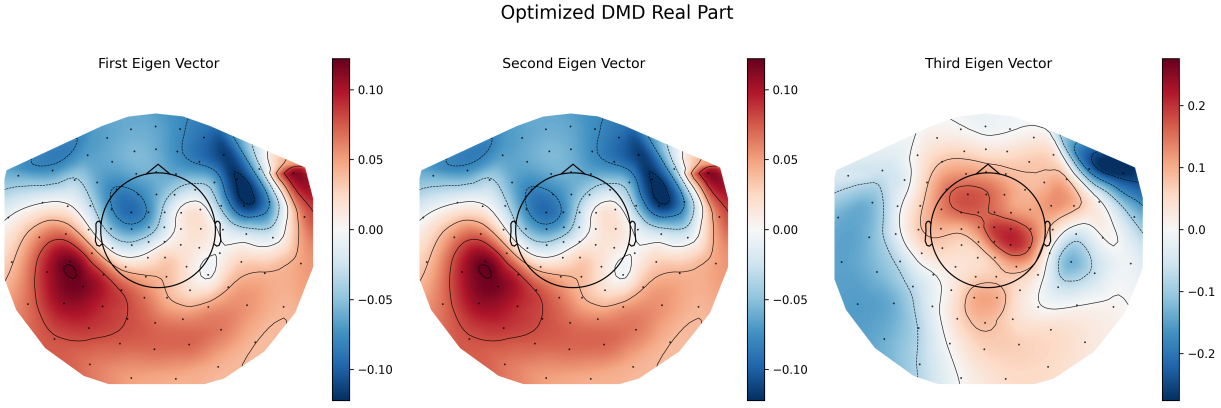

(b)

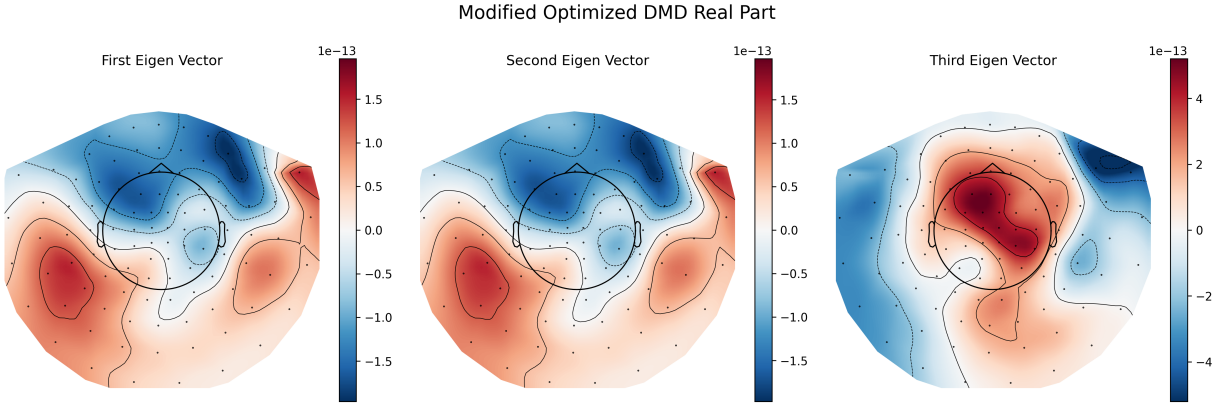

(c)

Figure 5.2: Comparison of the real part of the first three eigenvectors derived from the first MEG replicate using three different DMD algorithms: (a) Exact DMD, (b) Optimized DMD, and (c) Modified Optimized DMD. The real part of each eigenvector is shown. The colormap represents the amplitude of the eigenvectors, with red indicating positive and blue indicating negative values.

Chapter 6

CONCLUSIONS

This study demonstrates the promising performance of the Modified Optimized DMD method, which is a variation of Optimized DMD, across various noise settings. Specifically, Modified Optimized DMD outperformed both the Exact DMD and the Optimized DMD algorithms in estimating the real and imaginary parts of the eigenvalues, reducing both estimation error and empirical variance. The improvement was most notable among our medium uncorrelated and medium correlated noise settings and relatively minor among other noise settings. In MEG data analysis, both Optimized DMD and Modified Optimized DMD captured a more complex spatial and temporal pattern, compared to Exact DMD.

BIBLIOGRAPHY

Askham, T., & Kutz, J. N. (2018). Variable projection methods for an optimized dynamic mode decomposition. *SIAM Journal on Applied Dynamical Systems*, 17(1), 380–416. https://doi.org/10.1137/M1124176

Baddoo, P. J., Herrmann, B., McKeon, B. J., Kutz, J. N., & Brunton, S. L. (2023). Physics-informed dynamic mode decomposition. *Proceedings of the Royal Society A*, 479(20220576). http://doi.org/10.1098/rspa.2022.0576

Boto, E., Holmes, N., Leggett, J., Roberts, G., Shah, V., Meyer, S. S., Muñoz, L. D., Mullinger, K. J., Tierney, T. M., Bestmann, S., Barnes, G. R., Bowtell, R., & Brookes, M. J. (2018). Moving magnetoencephalography towards real-world applications with a wearable system [Epub 2018 Mar 21]. *Nature*, 555(7698), 657–661. https://doi.org/10.1038/nature26147

Brookes, M. J., Leggett, J., Rea, M., Hill, R. M., Holmes, N., Boto, E., & Bowtell, R. (2022). Magnetoencephalography with optically pumped magnetometers (opm-meg): The next generation of functional neuroimaging. *Trends in Neurosciences*, 45(8), 621–634.

Brunton, B. W., Johnson, L. A., Ojemann, J. G., & Kutz, J. N. (2016). Extracting spatial–temporal coherent patterns in large-scale neural recordings using dynamic mode decomposition. *Journal of neuroscience methods*, 258, 1–15.

Chen, K. K., Tu, J. H., & Rowley, C. W. (2012). Variants of dynamic mode decomposition: Boundary condition, koopman, and fourier analyses. *Journal of nonlinear science*, 22, 887–915.

Colbrook, M. J. (2023). The multiverse of dynamic mode decomposition algorithms. *arXiv preprint arXiv:2312.00137*.

Golub, G. H., & Pereyra, V. (1973). The differentiation of pseudo-inverses and nonlinear least squares problems whose variables separate. *SIAM Journal on numerical analysis*, 10(2), 413–432.

Groun, N., Villalba-Orero, M., Lara-Pezzi, E., Valero, E., Garicano-Mena, J., & Le Clainche, S. (2022). Higher order dynamic mode decomposition: From fluid dynamics to heart disease analysis. *Computers in Biology and Medicine*, 144, 105384. https://doi.org/https://doi.org/10.1016/j.compbiomed.2022.105384

Hemati, M. S., Rowley, C. W., Deem, E. A., & Cattafesta, L. N. (2017). De-biasing the dynamic mode decomposition for applied koopman spectral analysis of noisy datasets. *Theoretical and Computational Fluid Dynamics*, 31, 349–368.

Kutz, J., Brunton, S., Brunton, B., & Proctor, J. (2016). Dynamic mode decomposition: Data-driven modeling of complex systems. In *Dynamic mode decomposition: Data-driven modeling of complex systems* (p. 1). Society for Industrial; Applied Mathematics.

Li, C. Y., Chen, Z., Weerasuriya, A. U., Zhang, X., Lin, X., Zhou, L., Fu, Y., & Tse, T. K. (2023). Best practice guidelines for the dynamic mode decomposition from a wind engineering perspective. *Journal of Wind Engineering and Industrial Aerodynamics*, 241, 105506. https://doi.org/https://doi.org/10.1016/j.jweia.2023.105506

Tu, J. H. (2013). *Dynamic mode decomposition: Theory and applications* [Doctoral dissertation, Princeton University].

Appendix A

EFFECT OF DIFFERENT NOISE SETTINGS ON OTHER VARIABLES

Here we present the effect of different noise settings on the second and the third variables over time.

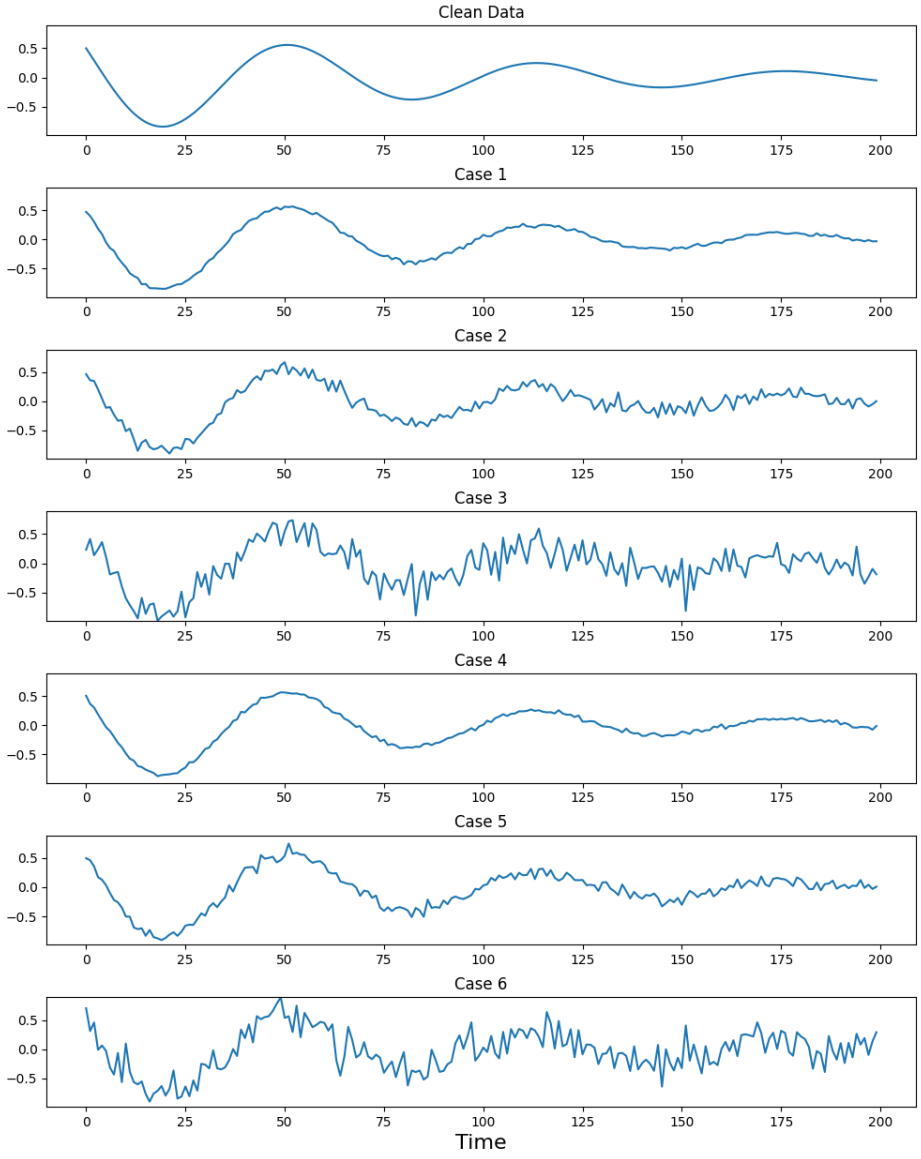

Figure A.1: Effect of different noise settings on the second variable over time. The first plot shows the clean data without any noise. Subsequent plots illustrate the impact of low, medium, and high levels of uncorrelated noise (Cases 1, 2, and 3), followed by the impact of low, medium, and high levels of correlated noise (Cases 4, 5, and 6).

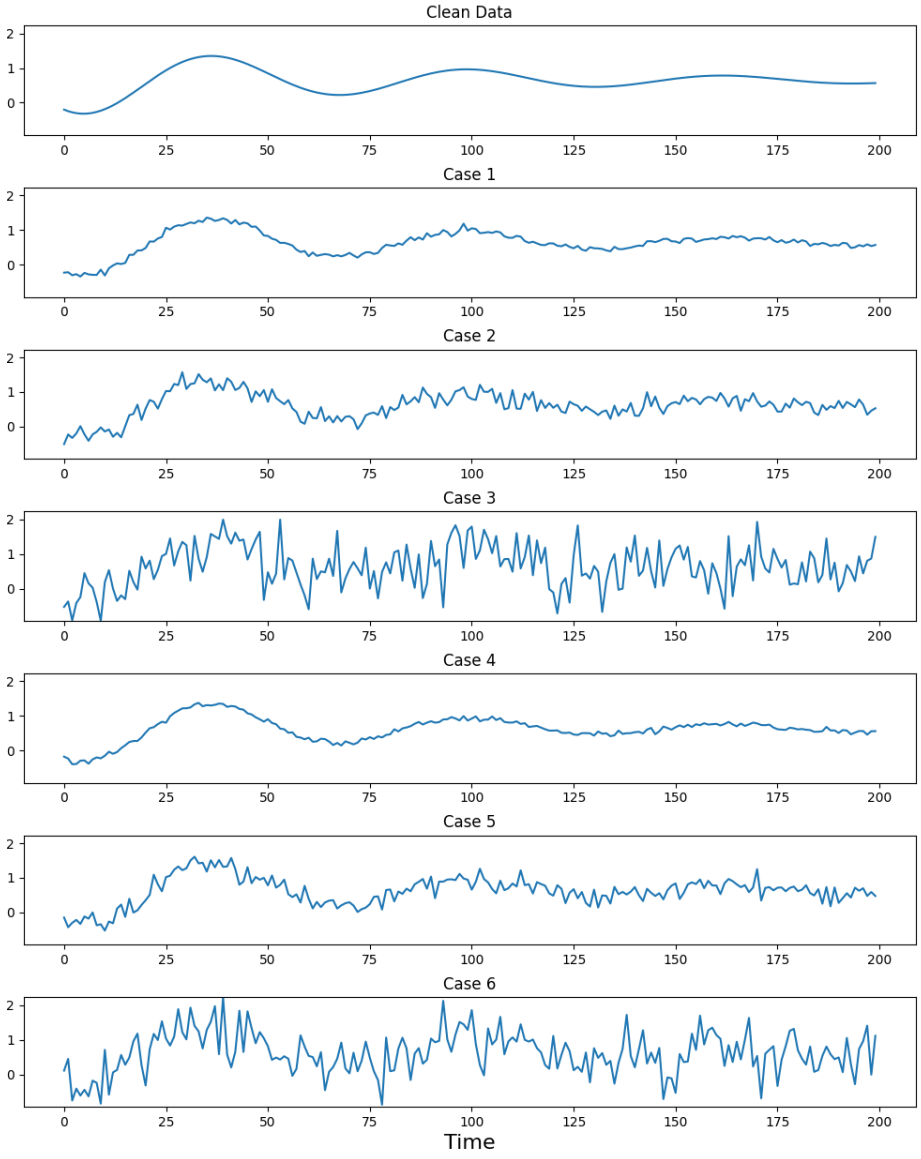

Figure A.2: Effect of different noise settings on the third variable over time. The first plot shows the clean data without any noise. Subsequent plots illustrate the impact of low, medium, and high levels of uncorrelated noise (Cases 1, 2, and 3), followed by the impact of low, medium, and high levels of correlated noise (Cases 4, 5, and 6).

Appendix B

RESULTS FROM OTHER SIMULATION SETTINGS

Here we present the results of the proposed simulation study across all simulation settings considered.

Variable	**Method**	**Bias**	**Empirical SD**	**MSE**
First	Exact	1.00×10^{-2}	1.10×10^{-3}	1.01×10^{-4}
	Optimized	1.13×10^{-4}	2.65×10^{-4}	8.27×10^{-8}
	Modified	1.12×10^{-4}	2.04×10^{-4}	5.39×10^{-8}
Second	Exact	-5.13×10^{-3}	7.50×10^{-4}	2.69×10^{-5}
	Optimized	1.14×10^{-4}	2.65×10^{-4}	8.30×10^{-8}
	Modified	1.12×10^{-4}	2.03×10^{-4}	5.39×10^{-8}
Third	Exact	-2.25×10^{-2}	7.50×10^{-4}	5.06×10^{-4}
	Optimized	-5.26×10^{-6}	2.93×10^{-4}	8.58×10^{-8}
	Modified	3.23×10^{-6}	2.20×10^{-4}	4.85×10^{-8}

Table B.1: Bias (Averaged Estimation Error), empirical standard deviation (SD), and mean squared error (MSE) for the real eigenvalues under low uncorrelated noise settings across different DMD algorithms.

Variable	Method	Bias	Empirical SD	MSE
First	Exact	8.51×10^{-4}	6.94×10^{-4}	1.21×10^{-6}
	Optimized	5.45×10^{-4}	3.97×10^{-4}	4.55×10^{-7}
	Modified	5.08×10^{-4}	2.80×10^{-4}	3.36×10^{-7}
Second	Exact	-8.51×10^{-4}	6.94×10^{-4}	1.21×10^{-6}
	Optimized	-5.43×10^{-4}	3.88×10^{-4}	4.45×10^{-7}
	Modified	-5.09×10^{-4}	2.82×10^{-4}	3.38×10^{-7}
Third	Exact	0	0	0
	Optimized	-2.16×10^{-6}	4.53×10^{-5}	2.06×10^{-9}
	Modified	7.95×10^{-7}	3.14×10^{-5}	9.87×10^{-10}

Table B.2: Bias (Averaged Estimation Error), empirical standard deviation (SD), and mean squared error (MSE) for the imaginary eigenvalues under low uncorrelated noise settings across different DMD algorithms.

Variable	Method	Bias	Empirical SD	MSE
First	Exact	-4.50×10^{-1}	1.09×10^{-1}	2.14×10^{-1}
	Optimized	5.33×10^{-4}	4.24×10^{-3}	1.83×10^{-5}
	Modified	5.38×10^{-4}	4.41×10^{-3}	1.98×10^{-5}
Second	Exact	-2.81×10^{-1}	3.93×10^{-2}	8.04×10^{-2}
	Optimized	8.69×10^{-4}	4.40×10^{-3}	2.01×10^{-5}
	Modified	9.03×10^{-4}	4.37×10^{-3}	1.99×10^{-5}
Third	Exact	-3.32×10^{-1}	8.32×10^{-2}	1.17×10^{-1}
	Optimized	-5.23×10^{-4}	2.55×10^{-3}	6.79×10^{-6}
	Modified	-3.48×10^{-4}	1.87×10^{-3}	3.63×10^{-6}

Table B.3: Bias (Averaged Estimation Error), empirical standard deviation (SD), and mean squared error (MSE) for the real eigenvalues under high uncorrelated noise settings across different DMD algorithms.

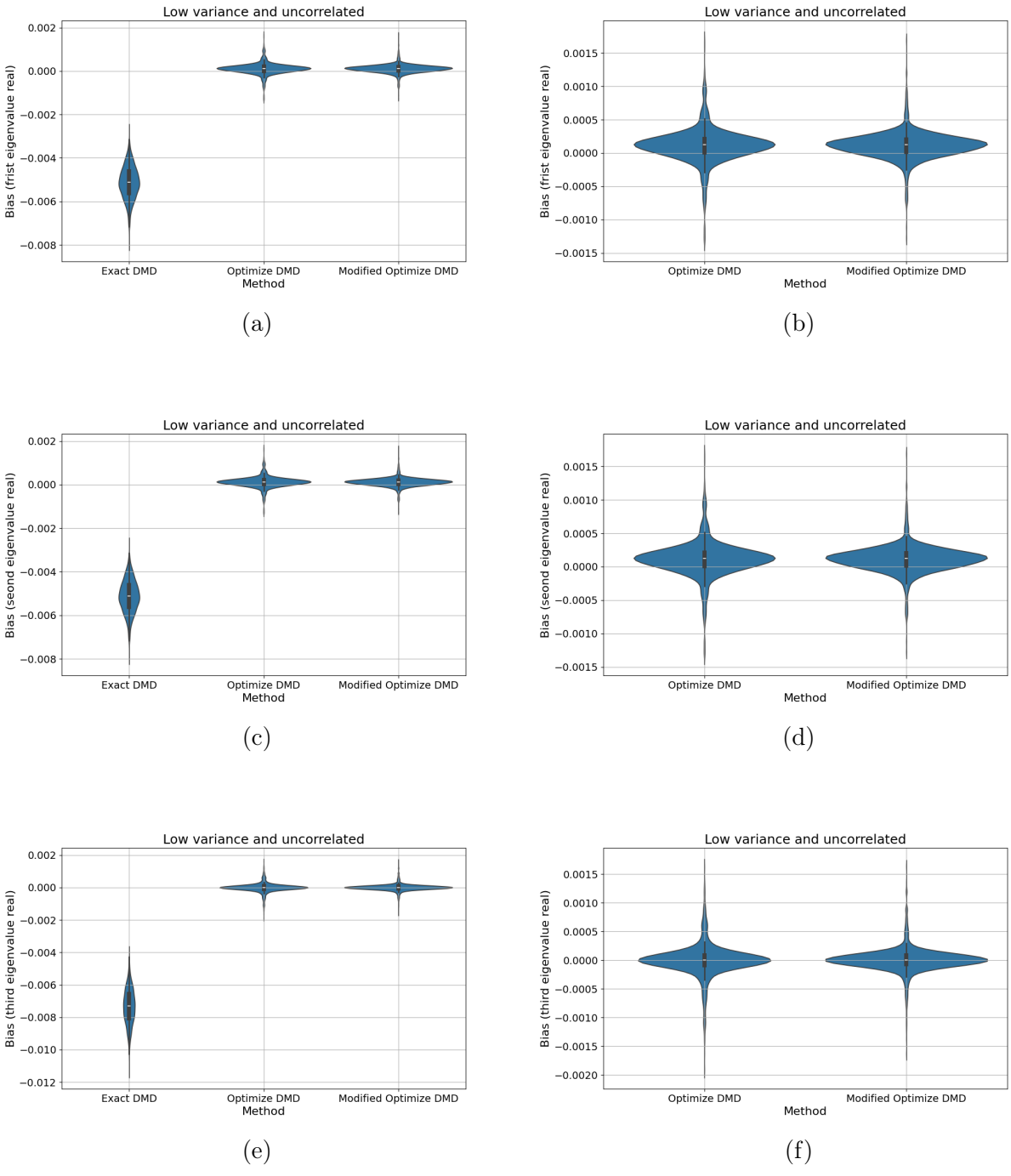

Figure B.1: Estimation error quantification for estimate of the eigenvalues' real parts under low variance and uncorrelated simulation setting. The violin plots illustrate the estimation error of the identified eigenvalues for Exact DMD, Optimize DMD, and Modified DMD methods. (a) and (b) show the estimation error distribution for the estimates of the real part of the first eigenvalue, (c) and (d) show the estimation error distribution for the estimated real part of the second eigenvalue, and (e) and (f) show the error distribution for the estimate of the real part of the third eigenvalue.

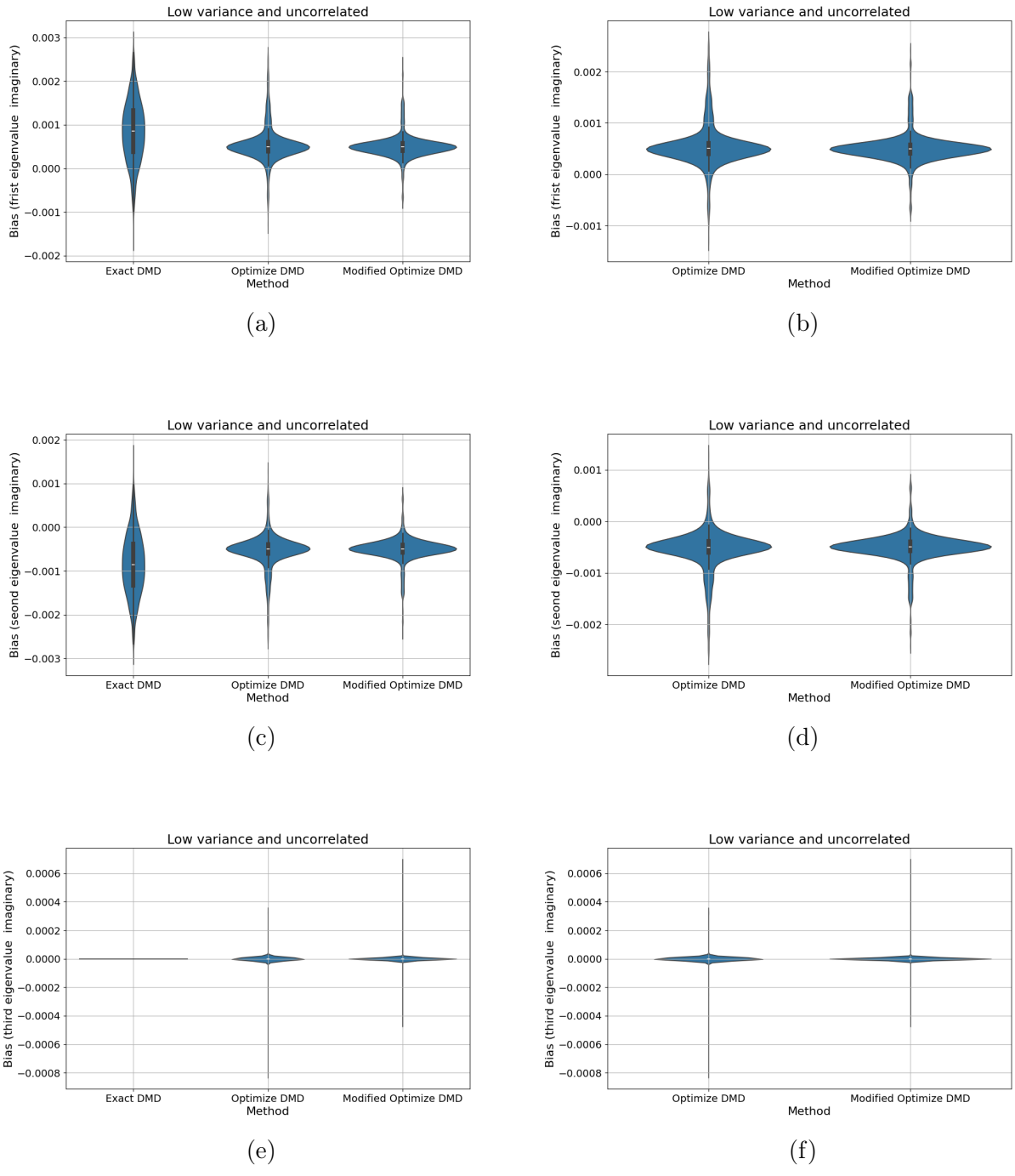

Figure B.2: Estimation error quantification for estimate of the eigenvalues' imaginary parts under low variance and uncorrelated simulation setting. The violin plots illustrate the estimation error of the identified eigenvalues for Exact DMD, Optimize DMD, and Modified DMD methods. (a) and (b) show the estimation error distribution for the estimates of the real part of the first eigenvalue, (c) and (d) show the estimation error distribution for the estimated real part of the second eigenvalue, and (e) and (f) show the error distribution for the estimate of the real part of the third eigenvalue.

Variable	Method	Bias	Empirical SD	MSE
First	Exact	6.06×10^{-2}	2.45×10^{-2}	4.27×10^{-3}
	Optimized	7.07×10^{-3}	1.52×10^{-2}	2.81×10^{-4}
	Modified	6.66×10^{-3}	1.58×10^{-2}	2.96×10^{-4}
Second	Exact	-9.76×10^{-2}	7.64×10^{-3}	9.59×10^{-3}
	Optimized	-8.68×10^{-3}	2.00×10^{-2}	4.76×10^{-4}
	Modified	-7.12×10^{-3}	1.74×10^{-2}	3.55×10^{-4}
Third	Exact	3.70×10^{-2}	2.49×10^{-2}	1.99×10^{-3}
	Optimized	1.69×10^{-3}	1.18×10^{-2}	1.42×10^{-4}
	Modified	6.04×10^{-4}	9.24×10^{-3}	8.57×10^{-5}

Table B.4: Bias (Averaged Estimation Error), empirical standard deviation (SD), and mean squared error (MSE) for the imaginary eigenvalues under high uncorrelated noise settings across different DMD algorithms.

Variable	Method	Bias	Empirical SD	MSE
First	Exact	9.78×10^{-3}	1.13×10^{-3}	9.69×10^{-5}
	Optimized	1.45×10^{-4}	2.84×10^{-4}	1.02×10^{-7}
	Modified	1.25×10^{-4}	2.10×10^{-4}	5.98×10^{-8}
Second	Exact	-5.09×10^{-3}	8.24×10^{-4}	2.66×10^{-5}
	Optimized	1.47×10^{-4}	2.84×10^{-4}	1.02×10^{-7}
	Modified	1.26×10^{-4}	2.10×10^{-4}	6.01×10^{-8}
Third	Exact	-2.24×10^{-2}	8.24×10^{-4}	5.04×10^{-4}
	Optimized	-2.42×10^{-5}	2.57×10^{-4}	6.67×10^{-8}
	Modified	-1.19×10^{-5}	1.87×10^{-4}	3.50×10^{-8}

Table B.5: Bias (Averaged Estimation Error), empirical standard deviation (SD), and mean squared error (MSE) for the real eigenvalues under low correlated noise settings across different DMD algorithms.

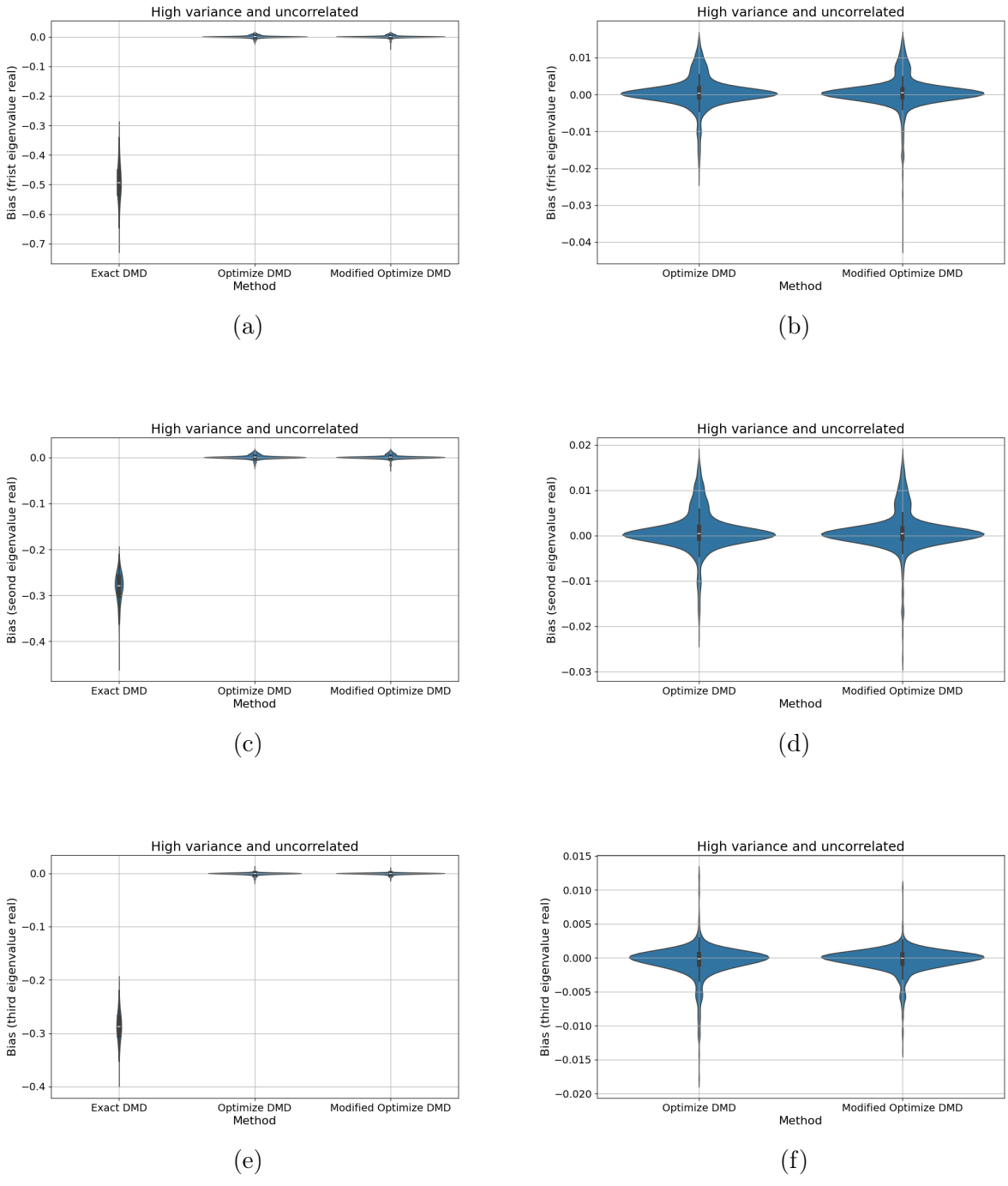

Figure B.3: Estimation error quantification for estimate of the eigenvalues' real parts under high variance and uncorrelated simulation setting. The violin plots illustrate the estimation error of the identified eigenvalues for Exact DMD, Optimize DMD, and Modified DMD methods. (a) and (b) show the estimation error distribution for the estimates of the real part of the first eigenvalue, (c) and (d) show the estimation error distribution for the estimated real part of the second eigenvalue, and (e) and (f) show the error distribution for the estimate of the real part of the third eigenvalue.

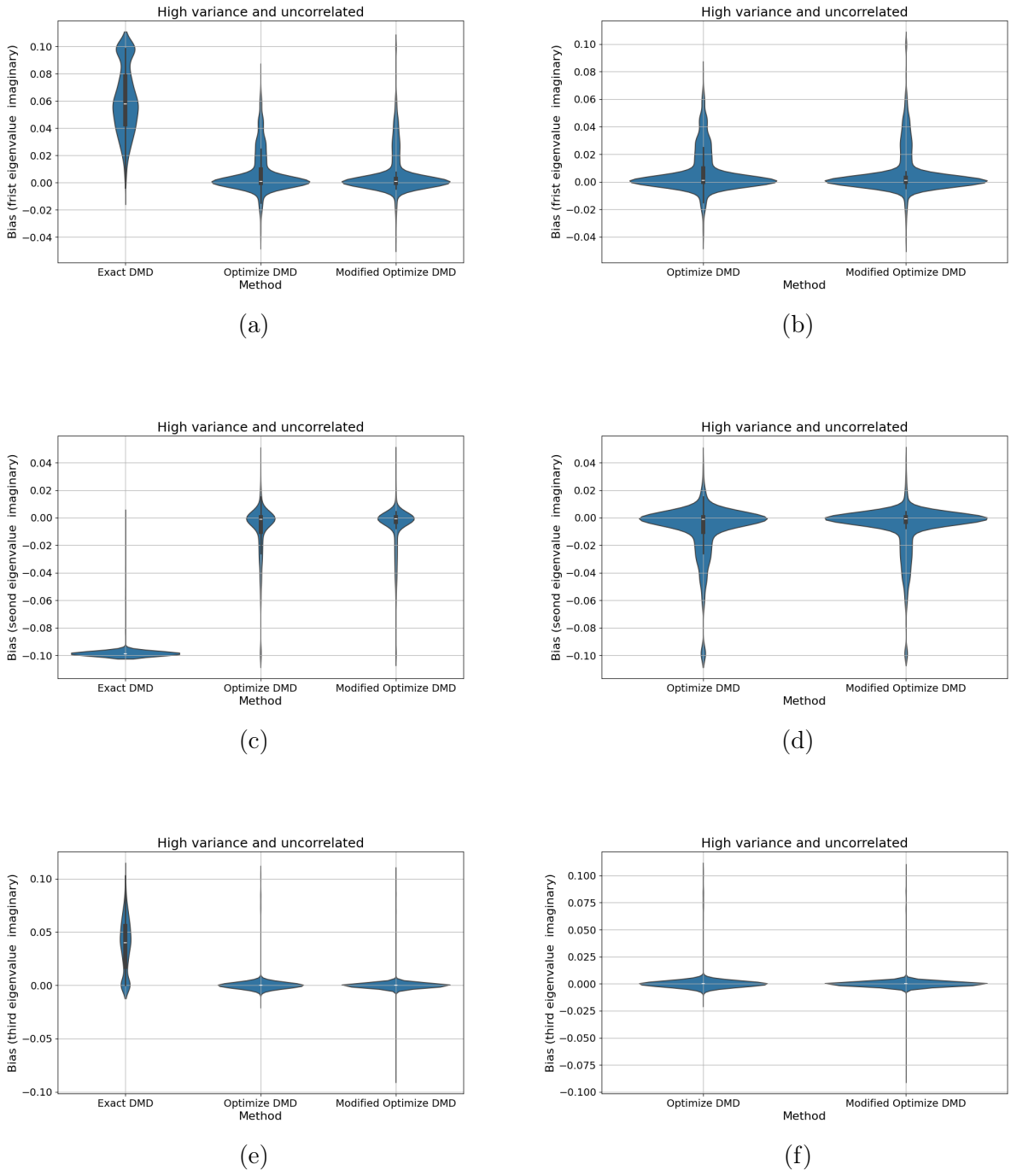

Figure B.4: Estimation error quantification for estimate of the eigenvalues' imaginary parts under high variance and uncorrelated simulation setting. The violin plots illustrate the estimation error of the identified eigenvalues for Exact DMD, Optimize DMD, and Modified DMD methods. (a) and (b) show the estimation error distribution for the estimates of the real part of the first eigenvalue, (c) and (d) show the estimation error distribution for the estimated real part of the second eigenvalue, and (e) and (f) show the error distribution for the estimate of the real part of the third eigenvalue.

Variable	Method	Bias	Empirical SD	MSE
First	Exact	1.16×10^{-3}	6.12×10^{-4}	1.72×10^{-6}
	Optimized	5.47×10^{-4}	3.35×10^{-4}	4.12×10^{-7}
	Modified	5.03×10^{-4}	2.29×10^{-4}	3.05×10^{-7}
Second	Exact	-1.16×10^{-3}	6.12×10^{-4}	1.72×10^{-6}
	Optimized	-5.44×10^{-4}	3.21×10^{-4}	3.99×10^{-7}
	Modified	-5.03×10^{-4}	2.24×10^{-4}	3.03×10^{-7}
Third	Exact	0	0	0
	Optimized	-3.82×10^{-6}	5.60×10^{-5}	3.16×10^{-9}
	Modified	-3.65×10^{-7}	3.58×10^{-5}	1.28×10^{-9}

Table B.6: Bias (Averaged Estimation Error), empirical standard deviation (SD), and mean squared error (MSE) for the imaginary eigenvalues under low correlated noise settings across different DMD algorithms.

Variable	Method	Bias	Empirical SD	MSE
First	Exact	-4.75×10^{-1}	1.28×10^{-1}	2.42×10^{-1}
	Optimized	7.54×10^{-4}	5.20×10^{-3}	2.76×10^{-5}
	Modified	6.23×10^{-4}	3.90×10^{-3}	1.56×10^{-5}
Second	Exact	-2.55×10^{-1}	2.90×10^{-2}	6.58×10^{-2}
	Optimized	1.19×10^{-3}	5.28×10^{-3}	2.93×10^{-5}
	Modified	9.80×10^{-4}	4.12×10^{-3}	1.80×10^{-5}
Third	Exact	-3.15×10^{-1}	1.07×10^{-1}	1.10×10^{-1}
	Optimized	-6.27×10^{-4}	2.49×10^{-3}	6.59×10^{-6}
	Modified	-4.05×10^{-4}	2.03×10^{-3}	4.27×10^{-6}

Table B.7: Bias (Averaged Estimation Error), empirical standard deviation (SD), and mean squared error (MSE) for the real eigenvalues under high correlated noise settings across different DMD algorithms.

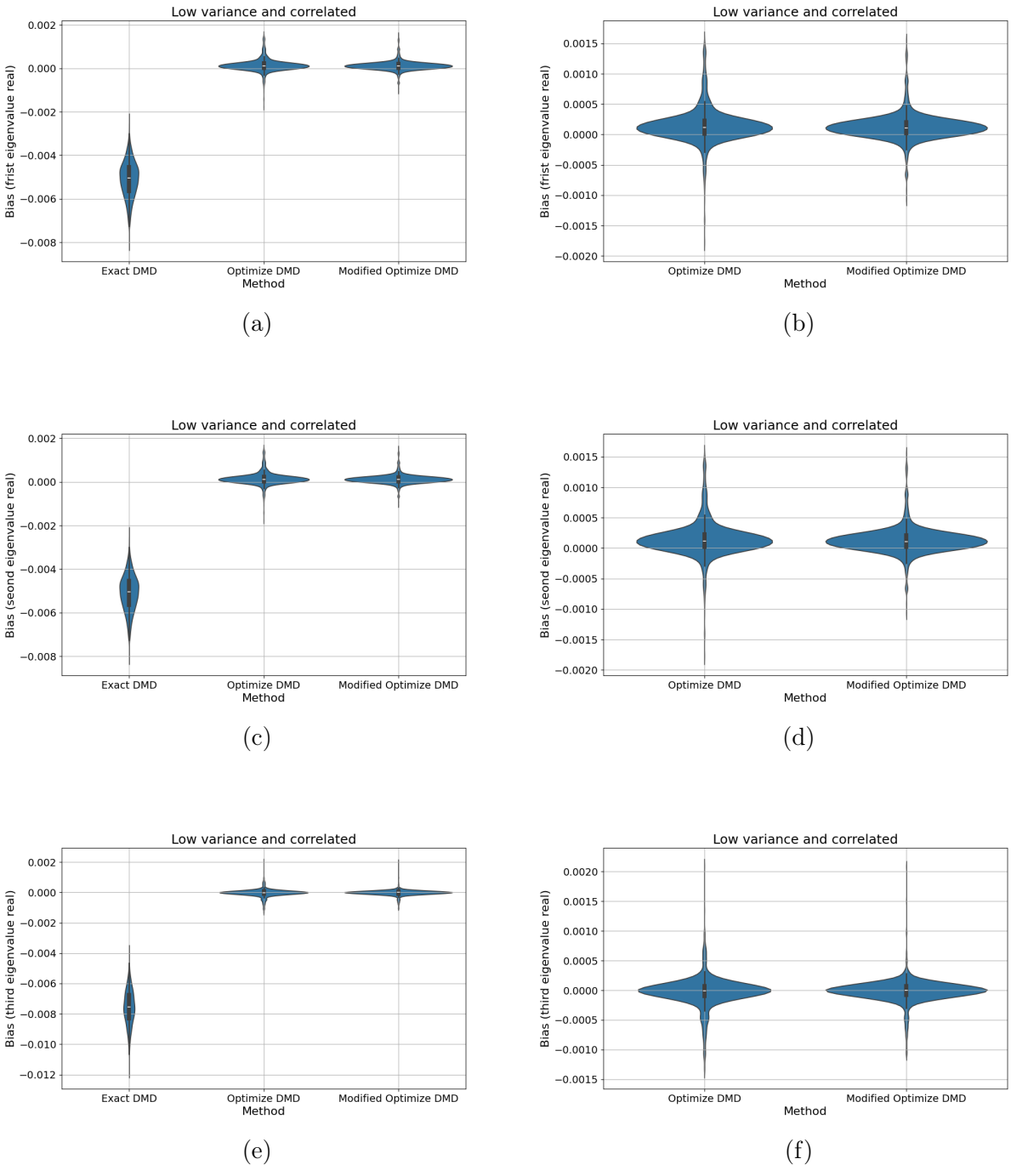

Figure B.5: Estimation error quantification for estimate of the eigenvalues' real parts under low variance and correlated simulation setting. The violin plots illustrate the estimation error of the identified eigenvalues for Exact DMD, Optimize DMD, and Modified DMD methods. (a) and (b) show the estimation error distribution for the estimates of the real part of the first eigenvalue, (c) and (d) show the estimation error distribution for the estimated real part of the second eigenvalue, and (e) and (f) show the error distribution for the estimate of the real part of the third eigenvalue.

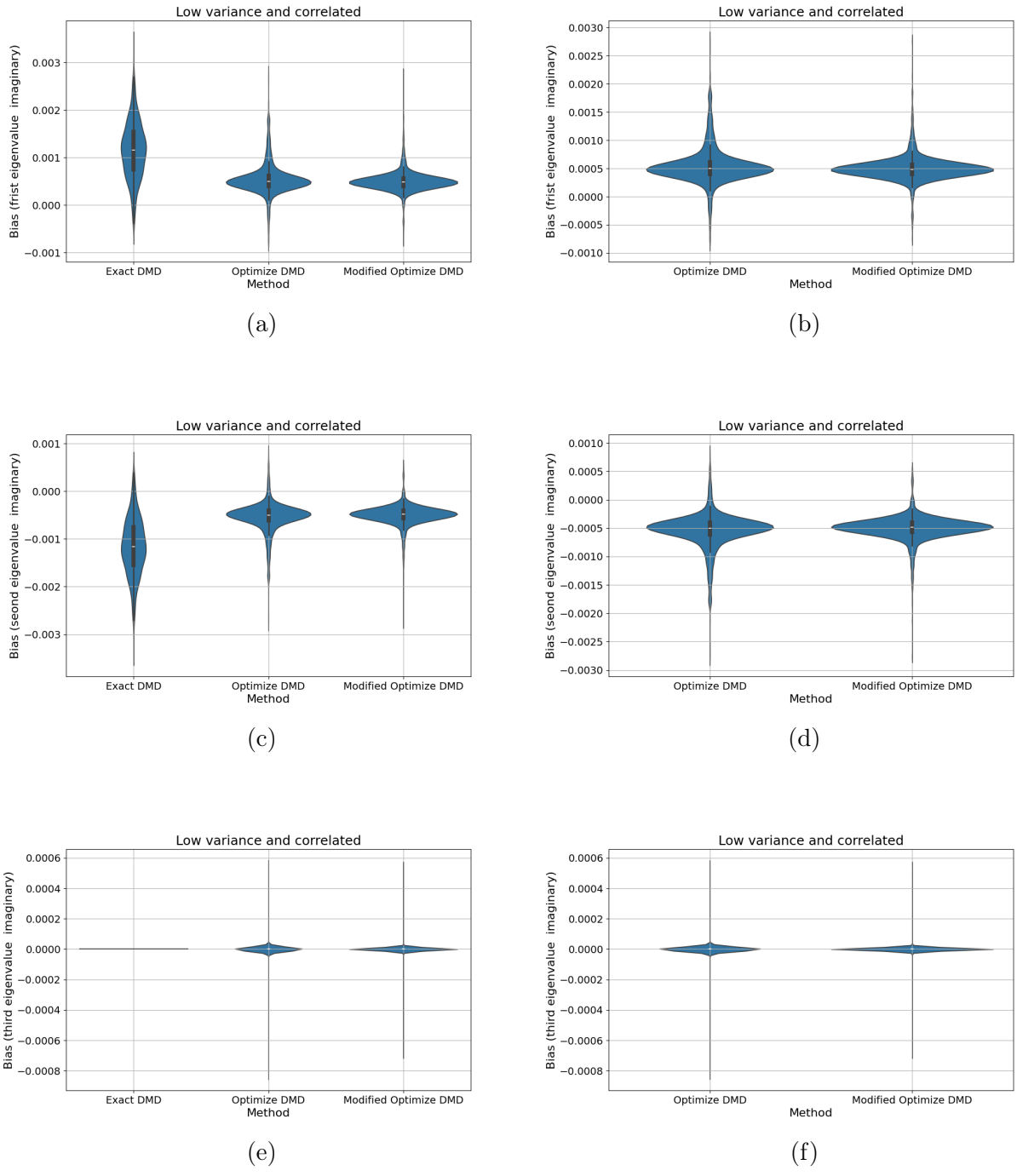

Figure B.6: Estimation error quantification for estimate of the eigenvalues' imaginary parts under low variance and correlated simulation setting. The violin plots illustrate the estimation error of the identified eigenvalues for Exact DMD, Optimize DMD, and Modified DMD methods. (a) and (b) show the estimation error distribution for the estimates of the real part of the first eigenvalue, (c) and (d) show the estimation error distribution for the estimated real part of the second eigenvalue, and (e) and (f) show the error distribution for the estimate of the real part of the third eigenvalue.

Variable	Method	Bias	Empirical SD	MSE
First	Exact	6.23×10^{-2}	2.36×10^{-2}	4.44×10^{-3}
	Optimized	6.02×10^{-3}	1.36×10^{-2}	2.21×10^{-4}
	Modified	4.60×10^{-3}	1.31×10^{-2}	1.93×10^{-4}
Second	Exact	-9.87×10^{-2}	0	9.74×10^{-3}
	Optimized	-8.01×10^{-3}	1.96×10^{-2}	4.47×10^{-4}
	Modified	-5.82×10^{-3}	1.75×10^{-2}	3.39×10^{-4}
Third	Exact	3.64×10^{-2}	2.36×10^{-2}	1.88×10^{-3}
	Optimized	1.98×10^{-3}	1.37×10^{-2}	1.92×10^{-4}
	Modified	1.21×10^{-3}	1.24×10^{-2}	1.56×10^{-4}

Table B.8: Bias (Averaged Estimation Error), empirical standard deviation (SD), and mean squared error (MSE) for the imaginary eigenvalues under high correlated noise settings across different DMD algorithms.

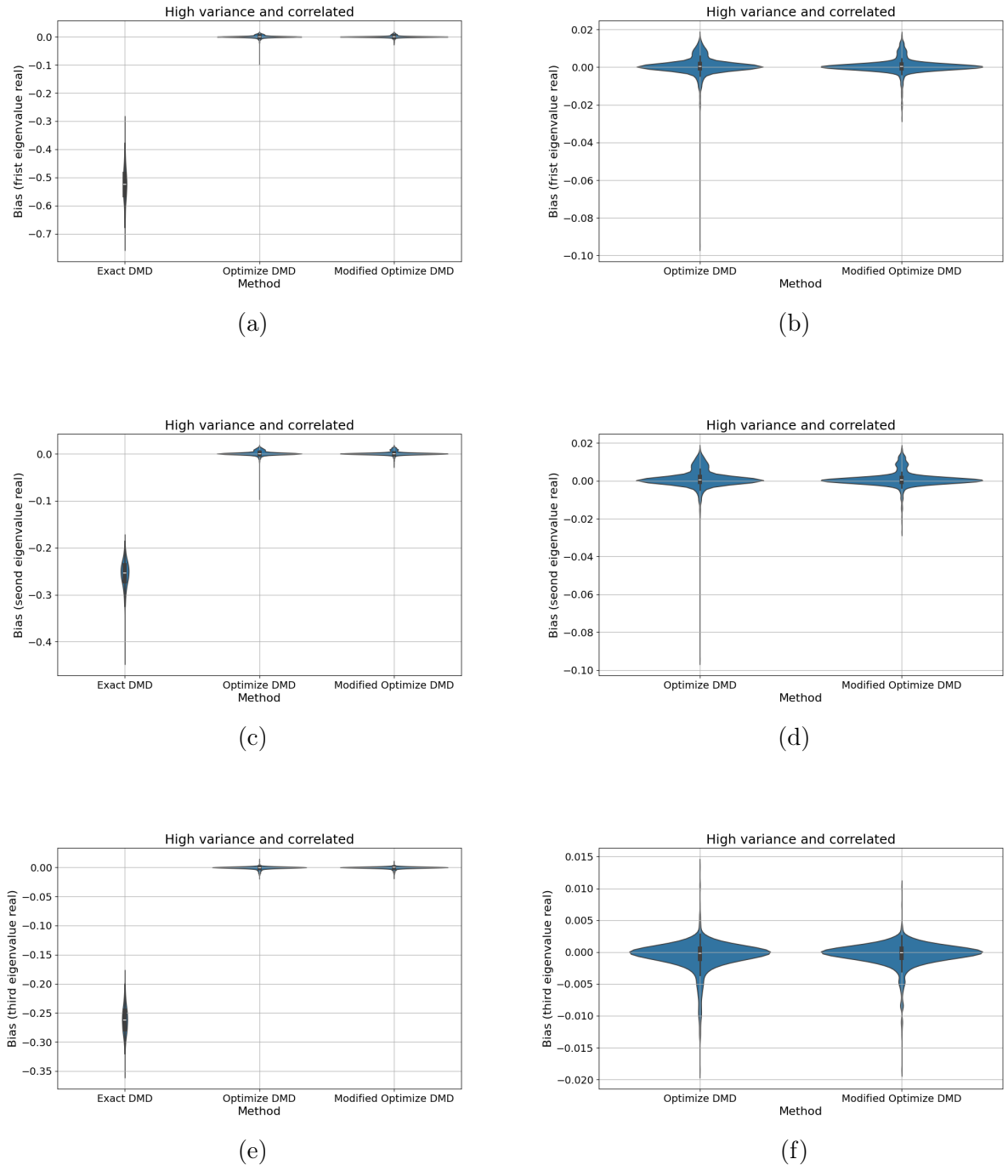

Figure B.7: Estimation error quantification for estimate of the eigenvalues' real parts under high variance and correlated simulation setting. The violin plots illustrate the estimation error of the identified eigenvalues for Exact DMD, Optimize DMD, and Modified DMD methods. (a) and (b) show the estimation error distribution for the estimates of the real part of the first eigenvalue, (c) and (d) show the estimation error distribution for the estimated real part of the second eigenvalue, and (e) and (f) show the error distribution for the estimate of the real part of the third eigenvalue.

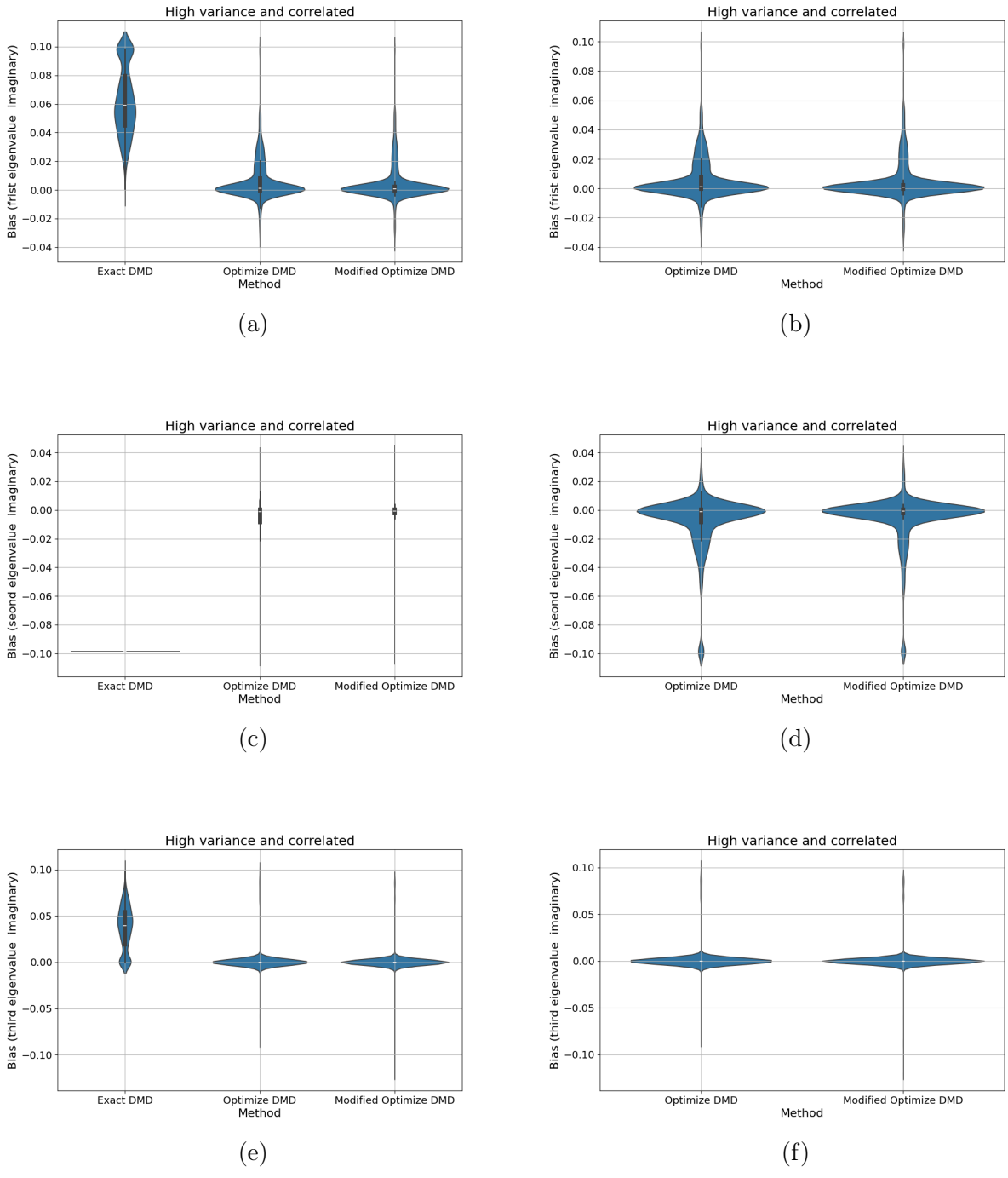

Figure B.8: Estimation error quantification for estimate of the eigenvalues' imaginary parts under high variance and correlated simulation setting. The violin plots illustrate the estimation error of the identified eigenvalues for Exact DMD, Optimize DMD, and Modified DMD methods. (a) and (b) show the estimation error distribution for the estimates of the real part of the first eigenvalue, (c) and (d) show the estimation error distribution for the estimated real part of the second eigenvalue, and (e) and (f) show the error distribution for the estimate of the real part of the third eigenvalue.